# Some Hybrid Methods in RCS Computation

Lei Wang

A Thesis

in

The Department

of

Electrical and Computer Engineering

Presented in Partial Fulfilment of the Requirements
for the Degree of Master of Applied Science at
Concordia University
Montreal, Quebec, Canada

February 2003

# ABSTRACT

Some Hybrid Methods in RCS Computation

Lei Wang

The RCS of wires, plates, plate/wire, plate/aperture, and plate/strip combinations were examined for plane wave incidence. In all cases, a NEC-2 (Numerical Electromagnetic Code, which is a Moment Method code) model was possible. Physical Optics (PO) also was used for RCS computation of the wire, plate/wire, and plate/aperture. For 2D TM scattering by a strip, Pulse Basis Point Matching (PBPM) and Asymptotic Phasefront Extraction (APE) were used to calculate the RCS and surface current density. Excellent RCS results were found by using only two pulse bases on a $20\lambda$ strip when APE was applied.

# ACKNOWLEDGEMENTS

The author wishes to thank his graduate supervisor Professor Robert Paknys for providing guidance, excellent suggestions, critical review of this thesis draft, and continuous financial support for the projects.

The author also wishes to thank Professor Ali Ghrayeb, Professor Mariana Frank and Professor Christopher W. Trueman for their participation in the examination committee and providing invaluable information both on the thesis draft as well as theoretical aspects.

# Table of Contents

# List of Figures

# Chapter 1

# Introduction

The search for solutions to Maxwell's Equations (ME) of electromagnetism has continued for more than a hundred years. For much of this time only the few relatively simple problems could be tackled for which analytical methods could be used. Lots of cases only become tractable if approximations or idealizations were made. In the last twenty years, asymptotic methods have been developed for treating scattering objects which are large in terms of wavelength. During the last decade, thanks to the new efficient and accurate numerical algorithms and the rapid development of computer hardware, the field of Computational Electromagnetics (CEM) has been in an expansion phase. The development of high-speed digital computers has allowed numerical methods to be applied to problems of almost arbitrary geometrical complexity. The problems that are treated by a CEM approach include radiation, scattering and Electromagnetic Compatibility (EMC) problems.

The most common scattering problem is to obtain the Radar Cross Section (RCS) of objects upon which electromagnetic fields impinge. The incident fields may be plane waves or non-planar fields from point sources, line sources, waveguides or other exciting elements. The RCS is calculated in the far field region, based on how much of the incident field is scattered in certain directions.

A common application of RCS calculations is to investigate how objects such as aircraft, ships or military vehicles scatter radar signals, and ultimately see how visible

the objects are to an observer. In order to minimize the scattered fields, numerical calculations can be employed to eliminate or lessen the need for live measurements.

There are two major approaches in CEM which can be identified. They represent fundamentally different ideas. The first one is Time-Domain (TD) methods which solve time-dependent partial differential equations at all frequencies, which can be resolved by the geometry by stepping forward in time and calculating how the fields propagate in each step. The other principle concerns Frequency-Domain (FD) methods, where you solve the fields for one frequency at a time and expand to all time by assuming they are time harmonic.

Furthermore, frequency-domain computations can be subdivided to two classes: the ray based methods and current based methods. The ray based techniques examine the behavior of rays along with their path. These rays are reflected by surfaces and diffracted by edges, wedges and possibly curved surfaces through various path. Geometrical Optics (GO), Geometrical Theory of Diffraction (GTD) and its modification Uniform Geometrical Theory of Diffraction (UTD) belong to this category. They are primarily high-frequency methods because they are used for the problems where the size of illuminated objects are large compared to the wavelength of the incident wave. When using current based methods, we first calculate the surface current induced on the objects illuminated by the incident fields, by solving Electric Field Integral Equation (EFIE) or Magnetic Field Integral Equation (MFIE). Then we can computer the scattered fields from the objects. The total field is the sum of the incident fields and scattered fields. The most common current based method is the Method of Moments (MoM or MM) which is an asymptotically exact integral equation method. An attractive alternative to MoM is the Physical Optics (PO) method, which is an approximate method. The description of all of these methods can be found in Balanis [1].

In the area of EMC, MoM [2]–[4] has been proved to be a powerful tool for the numerical computation of shielding effectiveness, coupling, or radiation from interfer-

ence sources. For plates and wires, the Numerical Electromagnetic Code (NEC-2) [5] is a widely used general purpose MoM code. However, the application of the MoM is limited to electrically small to medium sized bodies due to the strong dependence of CPU time and memory requirements on the frequency.

Hybrid methods combining the MoM with an asymptotic technique for the higher frequency range are well suited to overcome this difficulty. The application of current-based hybrid methods offers some advantages as compared to ray-based hybrid methods concerning the possible continuity of the surface current density at the boundary between the MoM- and the asymptotic region.

Current-based hybrid methods are usually based on PO [6], [7]. Due to the nature of the approximation, PO works best for large flat surfaces. It is viable since it is the one of the fastest method devised so far for simple objects.

Pulse Basis Point Matching (PBPM) method [8] is a solution of MoM. It is especially suitable for TM scattering by a strip. PBPM use pulse functions as basis functions, enforce the boundary condition to be true at matching points and use $\delta(x - x_m)$ functions as testing functions.

The PBPM solution requires small segments. Following Kwon et al. [9], we tried the Asymptotic Phasefront Extraction (APE) method, which includes a phase taper in the basis functions. The results shows the APE is more able to reproduce the rapidly varying surface current.

In this thesis, we try to gain some insight into the RCS and surface current computation by using some hybrid methods. Chapter 2 will give some theoretical foundations, which includes Maxwell's Equations (ME), Boundary Conditions (BC), the definition of Radar Cross Section (RCS), the Integral Equation, Moment Method (MoM) and Physical Optics Approximation (PO). Most of the material in Chapter 2 is described in Balanis [1], and it is provided as review and completeness.

In Chapter 3, we want to develop an understanding of what will happen to the

RCS of a large structure when other small obstacles are present. We describe the PO solution for wires, plates, and a wire/plate combination. This is compared with a NEC-2 model. We also studied the effect of holes in a plate, using PO. More interesting effects were observed by looking at a small vertical strip on the plate, which forms a dihedral reflector, by using NEC-2.

Chapter 4 of this thesis develops the theory and equations involved in the evaluation of RCS and surface current for TM scattering by a strip. Numerical results are presented. Comparisons were made with the results obtained by using PBPM and APE.

Chapter 5 presents the conclusions.

# Chapter 2

# Theoretical Foundation

This chapter describes the theoretical foundation and actual implementation of the Method of Moments (MoM) and the Physical Optics (PO). The topics covered in this chapter include explanations of basic concepts and derivation of the necessary equations. The details describing of MoM and PO can be found in Section 2.6 and Section 2.7. Most of the material in this chapter is described in Balanis[1], and it is provided here as review and completeness.

## 2.1 Maxwell's Equations (ME)

In general, electric and magnetic fields are vector quantities that have both magnitude and direction. The relations and variations of the electric and magnetic fields, charges, and currents associated with electromagnetic waves are governed by a set of coupled equations known as Maxwell's equations (ME).

$$\nabla \times \mathbf{E} = -\mathbf{M} - \frac{\partial \mathbf{B}}{\partial t} = -\mathbf{M} - \mu \frac{\partial \mathbf{H}}{\partial t} \tag{2.1}$$

$$\nabla \times \mathbf{H} = \mathbf{J} + \frac{\partial \mathbf{D}}{\partial t} = \mathbf{J} + \epsilon \frac{\partial \mathbf{E}}{\partial t} \tag{2.2}$$

$$\nabla \cdot \mathbf{E} = \frac{\rho_e}{\epsilon} \quad \text{or} \quad \nabla \cdot \mathbf{D} = \rho_e \tag{2.3}$$

$$\nabla \cdot \mathbf{H} = \frac{\rho_m}{\mu} \quad \text{or} \quad \nabla \cdot \mathbf{B} = \rho_m \tag{2.4}$$

$$\nabla \cdot \mathbf{J} = -\frac{\partial \rho_e}{\partial t} \tag{2.5}$$

$$\nabla \cdot \mathbf{M} = -\frac{\partial \rho_m}{\partial t} \tag{2.6}$$

where $\mathbf{J}$ and $\mathbf{M}$ are the electric and magnetic current densities, $\rho_e$ and $\rho_m$ are the electric and magnetic charge densities. Equations (2.1) through (2.6) are the ME in differential form. The differential form of ME is the most widely used representation to solve boundary-value electromagnetic problems.

The impressed (source) magnetic current density $\mathbf{M}$ and magnetic charge density $\rho_m$ have been introduced, respectively, in (2.1) and (2.4) through the "generalized" current concept. Although we have been accustomed to viewing magnetic charges and impressed magnetic current densities as not been physically realizable, they have been introduced to balance ME. Sometimes, equivalent magnetic charges and currents will be introduced to present physical problems. In addition, impressed magnetic current densities also can be considered as energy sources that generate the fields and whose field expression can be written in terms of these current densities. For some electromagnetic problems, their solution can often be aided by the introduction of "equivalent" impressed electric and magnetic current densities. The importance of both will become more obvious to some specific electromagnetic boundary-value problems.

ME is used to describe and relate the field vectors, current densities, and charge densities at any point in space at any time. ME in this form are valid for linear isotropic material in which the permeability is $\mu$ and the permittivity is $\epsilon$, both constant, and apply to all space. Field vectors associated with electromagnetic waves possess these characteristics except where there exist abrupt changes in charge and current densities. This means that ME can be limited to a smaller section of space by enforcing some boundary conditions (BC). Thus a complete description of the field vectors at any point at any time requires both ME and the associated BC.

ME in differential form for general time-varying electromagnetic fields were presented by (2.1) through (2.6). However, in many practical systems the time variations are of sinusoidal form and are referred to as *time-harmonic*. In general, such time

variations can be represented by $e^{j\omega t}$. Thus ME in differential form for time-harmonic fields can be written in terms of the complex field vectors as shown in (2.7) through (2.12)

$$\nabla \times \mathbf{E} = -\mathbf{M} - j\omega\mathbf{B} \tag{2.7}$$

$$\nabla \times \mathbf{H} = \mathbf{J} + j\omega\mathbf{D} \tag{2.8}$$

$$\nabla \cdot \mathbf{D} = \rho_e \tag{2.9}$$

$$\nabla \cdot \mathbf{B} = \rho_m \tag{2.10}$$

$$\nabla \cdot \mathbf{J} = -j\omega\rho_e \tag{2.11}$$

$$\nabla \cdot \mathbf{M} = -j\omega\rho_m \tag{2.12}$$

## 2.2 Boundary Conditions (BC)

As previously stated, the differential form of ME are used to solve for the field vectors provided the field quantities are single-valued, bounded, and possess (along with their derivatives) continuous distributions. Along boundaries where the media involved exhibit discontinuities in electrical properties (or there exist sources along these boundaries), the field vectors are also discontinuous and their behavior across the boundaries is governed by the *boundary conditions* (BC).

In General, BC can be expressed as

$$-\hat{\mathbf{n}} \times (\mathbf{E}_2 - \mathbf{E}_1) = \mathbf{M}_s \tag{2.13}$$

$$\hat{\mathbf{n}} \times (\mathbf{H}_2 - \mathbf{H}_1) = \mathbf{J}_s \tag{2.14}$$

$$\hat{\mathbf{n}} \cdot (\mathbf{D}_2 - \mathbf{D}_1) = \rho_{es} \tag{2.15}$$

$$\hat{\mathbf{n}} \cdot (\mathbf{B}_2 - \mathbf{B}_1) = \rho_{ms} \tag{2.16}$$

where $\hat{\mathbf{n}}$ denotes a vector normal to the surface of the interface and oriented from region 1 towards region 2, ($\mathbf{M}_s$, $\mathbf{J}_s$) and ($\rho_{es}$, $\rho_{ms}$) are the magnetic and electric linear (per meter) current and surface (per square meter) charge densities, respectively.

Equation (2.13) states that the tangential components of the electric field across an interface, along with there exists a surface magnetic current density $\mathbf{M}_s$, are discontinues by an amount equal to the magnetic current density. Similarly, (2.14) states that the tangential components of the magnetic field across an interface, along with there exists a surface electric current density $\mathbf{J}_s$, are discontinues by an amount equal to the electric current density. For normal components, (2.15) [(2.16)] states that the electric [magnetic] flux density on an interface along which a surface electric [magnetic] charge density resides are discontinues by an amount equal to the electric [magnetic] surface charge density.

If there is a source free space, then from BC we know that the tangential components of the electric and magnetic field intensities across an interface between two media are continuous. The normal components of the electric and magnetic field intensities are discontinuous, but the normal components of the electric and magnetic flux densities are continuous.

The BC for time-harmonic fields are identical to those general forms.

## 2.3 Radar Cross Section (RCS)

An important parameter in scattering studies is the electromagnetic scattering by a target which is usually represented by its echo area or *radar cross section* (RCS). RCS is defined as the area intercepting the amount of power that, when scattered isotropically, produces at the receiver a density that is equal to the density scattered by the actual target. For a two-dimensional target, the scattering parameter is referred to as the *scattering width* (SW) or alternatively as the RCS per unit length. In equation form the SW ($\sigma_{2-D}$) and RCS ($\sigma_{3-D}$) of a target takes the form of

$$\sigma_{2-D} = \lim_{\rho\to\infty}\left[2\pi\rho\frac{|\mathbf{E}_s|^2}{|\mathbf{E}_i|^2}\right] = \lim_{\rho\to\infty}\left[2\pi\rho\frac{|\mathbf{H}_s|^2}{|\mathbf{H}_i|^2}\right] \tag{2.17}$$

$$\sigma_{3-D} = \lim_{r\to\infty}\left[4\pi r^2\frac{|\mathbf{E}_s|^2}{|\mathbf{E}_i|^2}\right] = \lim_{r\to\infty}\left[4\pi r^2\frac{|\mathbf{H}_s|^2}{|\mathbf{H}_i|^2}\right] \tag{2.18}$$

where $\rho$, $r$ is the distance from target to observation point, $\mathbf{E}_s$, $\mathbf{H}_s$ are the scattered electric, magnetic fields and $\mathbf{E}_i$, $\mathbf{H}_i$ are the incident electric, magnetic fields, respectively. Since $|\mathbf{E}| = \eta|\mathbf{H}|$, then the $E$ ratios and $H$ ratios are the same.

## 2.4 Electrostatic Charge Distribution

From electrostatics we know that a linear electric charge distribution $\rho(\mathbf{r}')$ creates an electric potential, $V(\mathbf{r})$, which is

$$V(\mathbf{r}) = \frac{1}{4\pi\epsilon_0} \int_{\substack{source \\ (charge)}} \frac{\rho(\mathbf{r}')}{R} dl' \tag{2.19}$$

where $\mathbf{r}'(x', y', z')$ denotes the source coordinates, $\mathbf{r}(x, y, z)$ denotes the observation coordinates, $dl'$ is the path of integration, and R is the distance from any one point on the source to the observation point, which is generally represented by

$$R(r, r') = |\mathbf{r} - \mathbf{r}'| = \sqrt{(x - x')^2 + (y - y')^2 + (z - z')^2} \tag{2.19a}$$

We see that (2.19) may be used to calculate the potentials that are due to any known line charge density. However, the charge distribution on most configurations of practical interest is not usually known, even when the potential of the source is given. It is the nontrivial problem of determining the charge distribution that is to be solved here using integral equation numerical solution approach.

Consider a straight wire of length $l$ and radius $a$, placed along the $x$ axis, as shown in Fig. 2.1a. The wire is given a normalized constant electric potential of 1V. Choosing the observation along the wire axis, (2.19) can be expressed as

$$1 = \frac{1}{4\pi\epsilon_0} \int_0^l \frac{\rho(x')}{R(x, x')} dx' \qquad 0 \le x \le l \tag{2.20}$$

where

$$R(x, x') = R(r, r')|_{y=z=0} = \sqrt{(x - x')^2 + (y')^2 + (z')^2} = \sqrt{(x - x')^2 + a^2} \tag{2.20a}$$

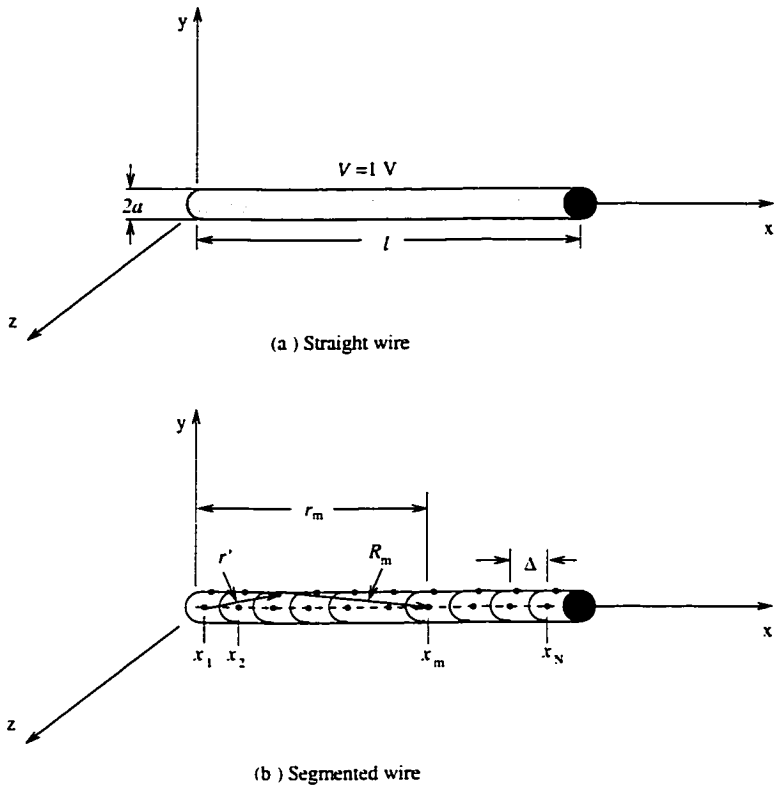


Figure 2.1: Constant potential straight wire of length $l$ and radius $a$. and the segmentation of the wire [1].

Equation (2.20) is an integral equation that can be used to find the charge density $\rho(x')$ based on the 1-V potential. The solution may be reached numerically by reducing (2.20) to a series of linear algebraic equation that may be solved by conventional matrix equation techniques. To facilitate this, let us approximate the unknown charge distribution $\rho(x')$ by an expansion of $N$ known terms with constant, but unknown coefficients, that is,

$$\rho(x') = \sum_{n=1}^{N} a_n g_n(x') \tag{2.21}$$

Thus, (2.20) may be written as

$$4\pi\epsilon_0 = \int_0^l \frac{1}{R(x,x')} \left[ \sum_{n=1}^{N} a_n g_n(x') \right] dx' \tag{2.22}$$

Because (2.22) is a nonsingular integral, its integration and summation can be

interchanged, and it can be written as

$$4\pi\epsilon_0 = \sum_{n=1}^{N} a_n \int_0^l \frac{g_n(x')}{\sqrt{(x-x')^2+a^2}} dx' \tag{2.23}$$

The wire is now divided into $N$ uniform segments, each of length $\Delta = l/N$, as illustrated in Fig. 2.1b. The $g_n(x')$ functions in the expansion (2.21) are chosen for their ability to accurately model the unknown quantity, while minimizing computation. They are often referred to as *basis* functions.

## 2.5 Integral Equation

Equation (2.20) for the 1-V potential on a wire of length $l$ is an integral equation, which can be used to solve for the charge distribution. Numerically this is accomplished using a method, which is usually referred to as *Moment Method* or *Method of Moments* (MoM).

Equation (2.20) is valid at every point on the wire. By enforcing (2.20) at $N$ discrete but different points on the wire, $x = x_m, m = 1, 2, ...n$, the integral equation of (2.20) is reduced to a set of $N$ linearly independent algebraic equations

$$[V_m] = [Z_{mn}][I_n] \tag{2.24}$$

where

$$Z_{mn} = \int_0^l \frac{g_n(x')}{\sqrt{(x_m-x')^2+a^2}} dx' \tag{2.24a}$$

$$I_n = a_n \tag{2.24b}$$

$$V_m = 4\pi\epsilon_0 \tag{2.24c}$$

which is solved for the unknown coefficient $a_n$ by using matrix inversion techniques. Since the system of $N$ linear equations each with $N$ unknowns was derived by applying the boundary condition (constant 1-V potential) at $N$ discrete points on the wire, the technique is referred to as *point-matching* (or *collocation*) method.

In general, there are many forms of integral equations. For time-harmonic electromagnetics, two of the most popular integral equations are the *electric field integral equation* (EFIE) and the *magnetic field integral equation* (MFIE). The EFIE enforces the boundary condition on the tangential electric field, and is valid for both closed or open surfaces. Meanwhile the MFIE enforces the boundary condition on the tangential components of the magnetic field, and is valid for closed surfaces only. These integral equations can be used for both radiation and scattering problems. Two popular EFIEs are the Pocklington Integral Equation and the Hallén Integral Equation.

### 2.5.1 Pocklington's Integral Equation

Let us assume that an incident wave impinges on the surface of a conducting wire, as shown in Fig. 2.2a, and it is referred to as the *incident electric field* $\mathbf{E}^i(\mathbf{r})$. Part of the incident field impinges on the wire and induces a linear current density $\mathbf{J}_s$. The induced current density $\mathbf{J}_s$ reradiates and produces an electric field that is referred to as the *scattered electric field* $\mathbf{E}^s(\mathbf{r})$. Therefore, at any point in space, the total electric field $\mathbf{E}^t(\mathbf{r})$ is the sum of the incident and scattered fields, or

$$\mathbf{E}^t(\mathbf{r}) = \mathbf{E}^i(\mathbf{r}) + \mathbf{E}^s(\mathbf{r}) \tag{2.25}$$

According to boundary condition, on the surface of the wire ($r = r_s$), the total tangential electric field (here it is $E_z$) should vanish. Therefore we have

$$E_z^t(r = r_s) = E_z^i(r = r_s) + E_z^s(r = r_s) \tag{2.26}$$

or

$$E_z^s(r = r_s) = -E_z^i(r = r_s) \tag{2.26a}$$

In general, the scattered electric field generated by the induced current density $\mathbf{J}_s$ can be expressed as

$$\mathbf{E}^s(\mathbf{r}) = -j\omega\mathbf{A} - j\frac{1}{\omega\mu\epsilon}\nabla(\nabla\cdot\mathbf{A}) = -j\frac{1}{\omega\mu\epsilon}[k^2\mathbf{A} + \nabla(\nabla\cdot\mathbf{A})] \tag{2.27}$$

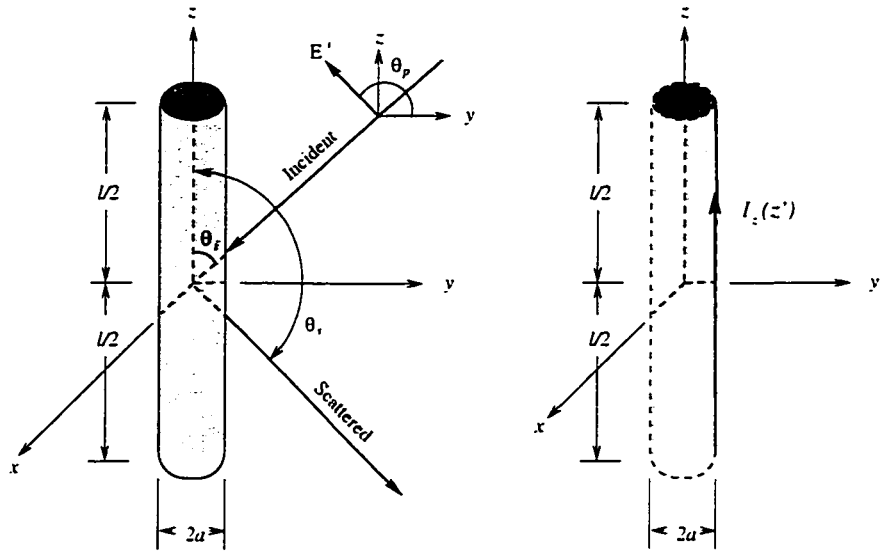


Figure 2.2: Uniform plane wave obliquely incident on a $z$ directed conducting wire [1].

where $\mathbf{A}$ is the magnetic vector potential, and it satisfies

$$\nabla^2 \mathbf{A} + k^2 \mathbf{A} = -\mu \mathbf{J}_s \tag{2.28}$$

However, at the wire surface, only the $z$ component is needed, so we have

$$E_z^s(r) = -j\frac{1}{\omega\mu\epsilon}\left(k^2 A_z + \frac{\partial^2 A_z}{\partial z^2}\right) \tag{2.29}$$

According to the solution of the vector potential wave equations, for a linear current density $\mathbf{J}_s$, we can obtain $\mathbf{A}$ like this

$$\mathbf{A} = \frac{\mu}{4\pi}\iint_S \mathbf{J}_s \frac{e^{-jkR}}{R} ds' \tag{2.30}$$

Then, the $z$ component is

$$A_z = \frac{\mu}{4\pi}\iint_S J_z \frac{e^{-jkR}}{R} ds' = \frac{\mu}{4\pi}\int_{-l/2}^{l/2}\int_0^{2\pi} J_z \frac{e^{-jkR}}{R} a d\phi' dz' \tag{2.31}$$

If the wire is very thin, the current density $J_z$ can be written as

$$J_z = \frac{1}{2\pi a} I_z(z') \tag{2.32}$$

where $I_z(z')$ is assumed to be an equivalent filament line-source current located a radial distance $\rho = a$ from the $z$ axis, as shown in Fig. 2.2b. Thus (2.31) reduces to

$$A_z = \frac{\mu}{4\pi}\int_{-l/2}^{l/2}\int_0^{2\pi} I_z(z')\frac{e^{-jkR}}{2\pi R}d\phi' dz' \tag{2.33}$$

where

$$\begin{aligned} R &= \sqrt{(x-x')^2+(y-y')^2+(z-z')^2} \\ &= \sqrt{\rho^2+a^2-2\rho a\cos(\phi-\phi')+(z-z')^2} \end{aligned} \tag{2.33a}$$

Because of symmetry of the scatterer, we choose $\phi = 0$. Then for observation on the surface $\rho = a$ of the scatterer, (2.33) and (2.33a) reduce to

$$\begin{aligned} A_z(\rho=a) &= \mu\int_{-l/2}^{l/2} I_z(z')\left(\frac{1}{2\pi}\int_0^{2\pi}\frac{e^{-jkR}}{4\pi R}d\phi'\right)dz' \\ &= \mu\int_{-l/2}^{l/2} I_z(z')G(z,z')dz' \end{aligned} \tag{2.34}$$

where

$$G(z,z') = \frac{1}{2\pi}\int_0^{2\pi}\frac{e^{-jkR}}{4\pi R}d\phi' \tag{2.34a}$$

$$R(\rho=a) = \sqrt{4a^2\sin^2\left(\frac{\phi'}{2}\right)+(z-z')^2} \tag{2.34b}$$

Thus, the $z$ component of the scattered electric field can be expressed as

$$E_z^s(\rho=a) = -j\frac{1}{\omega\epsilon}\left(k^2+\frac{\partial^2}{\partial z^2}\right)\int_{-l/2}^{l/2} I_z(z')G(z,z')dz' \tag{2.35}$$

which by using (2.26a) reduces to

$$-j\frac{1}{\omega\epsilon}\left(k^2+\frac{\partial^2}{\partial z^2}\right)\int_{-l/2}^{l/2} I_z(z')G(z,z')dz' = -E_z^i(\rho=a) \tag{2.36}$$

Exchanging integration with differentiation, we can rewrite (2.36) as

$$\int_{-l/2}^{l/2} I_z(z')\left[\left(\frac{\partial^2}{\partial z^2}+k^2\right)G(z,z')\right]dz' = -j\omega\epsilon E_z^i(\rho=a) \tag{2.37}$$

where $G(z,z')$ is given by (2.34a).

Equation (2.37) is referred to as *Pocklington's integral equation.* By knowing the incident field on the surface of the wire, (2.37) can be used to determine the equivalent filamentary line-source current of the wire, and thus current density on the wire.

If we assume that the wire is very thin ($a \ll \lambda$) such that (2.34a) reduces to

$$G(z, z') = G(R) = \frac{e^{-jkR}}{4\pi R} \tag{2.38}$$

then (2.37) can be expressed in a more convenient form as

$$\int_{-l/2}^{l/2} I_z(z') \frac{e^{-jkR}}{4\pi R^5} \left[(1 + jkR)(2R^2 - 3a^2) + (kaR)^2\right] dz' = -j\omega\epsilon E_z^i(\rho = a) \tag{2.39}$$

where for observations along the center of the wire ($\rho = 0$)

$$R = \sqrt{a^2 + (z - z')^2} \tag{2.39a}$$

In (2.37) or (2.39), $I_z(z')$ represents the equivalent filamentary line-source current located on the surface of the wire, as shown in Fig. 2.2b, and it is obtained by knowing the incident electric field on the surface of the wire.

### 2.5.2 Hallén's Integral Equation

Referring again to Fig. 2.2a, let us assume that the length of the cylinder is much larger than its radius ($l \gg a$) and its radius is much smaller than the wavelength ($a \ll \lambda$) so that the effect of the end faces of the cylinder can be neglected. Therefore the boundary conditions for a wire with infinite conductivity are those of vanishing total tangential **E** fields on the surface of the cylinder and vanishing current at the ends of the cylinder.

Since only an electric current density flows on the cylinder and it is directed along the $z$ axis ($\mathbf{J}_s = \hat{\mathbf{z}} J_z$), then according (2.28) and (2.30), $\mathbf{A} = \hat{\mathbf{z}} A_z(z')$, which is only a function of $z'$ for small radii. Thus (2.26) reduces to

$$E_z^t = -j\frac{1}{\omega\mu\epsilon}\left(k^2 A_z + \frac{\partial^2 A_z}{\partial z^2}\right) \tag{2.40}$$

Applying the boundary condition, the total tangential electric field $E_z^t$ vanishes on the surface of the cylinder, (2.40) reduces to

$$k^2 A_z + \frac{\partial^2 A_z}{\partial z^2} = 0 \tag{2.40a}$$

The current density on the cylinder is symmetrical, so is the potential $A_z$. Thus the solution of (2.40a) is given by

$$A_z(z) = -j\sqrt{\mu\epsilon}[B_1 \cos(kz) + C_1 \sin(k|z|)] \tag{2.41}$$

where $B_1$ and $C_1$ are constant. For a current-carrying wire, its potential $A$ is given by

$$\mathbf{A} = \frac{\mu}{4\pi} \iint_C \mathbf{I} \frac{e^{-jkR}}{R} dl' \tag{2.42}$$

so we have

$$A_z(z) = \frac{\mu}{4\pi} \int_{-l/2}^{l/2} I_z(z') \frac{e^{-jkR}}{R} dz' \tag{2.43}$$

Equating (2.43) to (2.41) leads to

$$\int_{-l/2}^{l/2} I_z(z') \frac{e^{-jkR}}{4\pi R} dz' = -j\sqrt{\frac{\epsilon}{\mu}}[B_1 \cos(kz) + C_1 \sin(k|z|)] \tag{2.44}$$

Equation (2.44) is referred to as *Hallén's integral equation* for a perfectly conducting wire.

## 2.6 Moment Method Solution (MoM)

Equation (2.37), (2.39) and (2.44) each has the form of

$$F(g) = h \tag{2.45}$$

where $F$ is a known linear operator, $h$ is a known excitation function, and $g$ is the response function. The objective here is to determine $g$ once $F$ and $h$ are specified.

Moment method requires that the unknown response function be expanded as a linear combination of $N$ terms and written as

$$g(z') = \sum_{n=1}^{N} a_n g_n(z') \tag{2.46}$$

Each $a_n$ is an unknown constant and each $g_n(z')$ is a known function usually referred to as a *basis function*. So in other words, $g(z')$ can be expanded in terms of a finite series of known basis functions with unknown amplitudes. Substituting (2.46) into (2.45) and using the linearity of the $F$ operator reduces (2.45) to

$$\sum_{n=1}^{N} a_n F(g_n) = h \tag{2.47}$$

Expansion of (2.47) leads to one equation with $N$ unknowns. To resolve the $N$ constants, it is necessary to have $N$ linearly independent equations. This can be done by applying boundary condition at $N$ different points (point-matching), just like we have done in Section 2.4. Doing this, (2.47) takes the form of

$$\sum_{n=1}^{N} a_n F(g_n) = h_m \qquad\qquad m = 1, 2, ..., N \tag{2.48}$$

In matrix form, (2.48) can be expressed as

$$[Z_{mn}][I_n] = [V_m] \tag{2.49}$$

where

$$Z_{mn} = F(g_n) \tag{2.49a}$$

$$I_n = a_n \tag{2.49b}$$

$$V_m = h_m \tag{2.49c}$$

The unknown coefficients $a_n$ can be found by solving (2.49) using matrix inversion techniques, or

$$[I_n] = [Z_{mn}]^{-1}[V_m] \tag{2.50}$$

### 2.6.1 Basis Functions

One very important step in MoM is the choice of basis functions. The basis functions $g_n$ are chosen so that each $F(g_n)$ in (2.47) can be evaluated conveniently. They should

accurately represent and resemble the anticipated unknown function, meanwhile minimizing the computational effort.

There are many possible sets of basis functions. They may be divided into two general classes: *subdomain functions* and *entire domain functions.*

*A. Subdomain Functions*

Of the two types of basis functions, subdomain functions are the most common, because they may be used without prior knowledge of the nature of the function that they must represent. Also, in order to deal with bent wires and arbitrarily shaped wire meshes, it is more useful to divide the wires up into a series of short segments and define a set of functions each of which is non-zero over a few segments only.

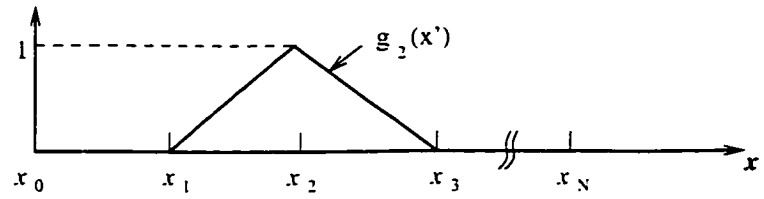


(a) Single

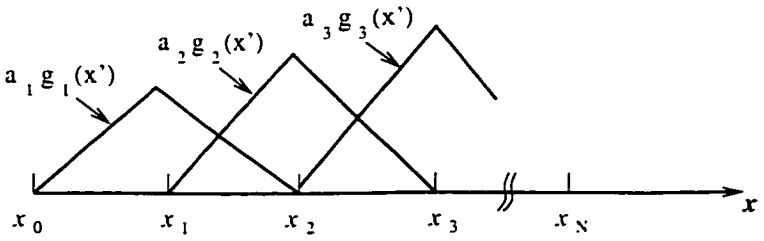


(b) Multiple

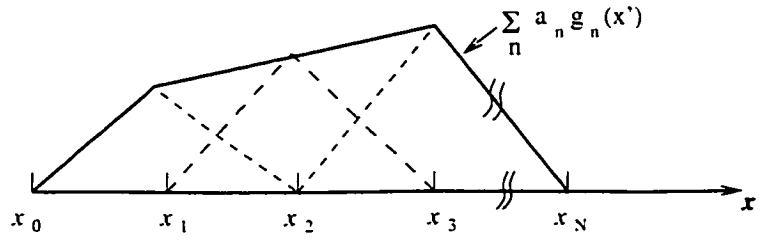


(c) Function representation

Figure 2.3: Piecewise linear approximation to current for subdomain functions in Moment Method solution [1].

To illustrate the method, overlapping triangle functions are chosen because they lead to a piecewise-linear approximation to the current and yet are relatively simple. As shown in Fig. 2.3a, each triangle function, $g_n$, is based on two segments and overlaps its neighbor by one segment. It is of unit height. Thus, the current is expanded as

$$g(x') = \sum_{n=1}^{N} a_n g_n(x') \tag{2.51}$$

where $N$ is the number of triangle functions needed to cover the wires. In this way a piecewise-linear approximation to the currents is obtained, as depicted in Fig. 2.3c. The amplitudes $a_n$ are the unknowns which need to be found.

Other commonly used basis functions are pulse (step) functions, sinusoidal functions, truncated cosine functions, or a three-term function (consisting of constant, sine and cosine terms) as used in NEC.

*B. Entire Domain Functions*

Entire domain basis functions, as their name implies, are defined and are nonzero over the entire length of the structure being considered. Thus no segmentation is involved. Because we are constrained to use a finite number of functions, entire domain basis functions usually have difficulty in modeling arbitrary or complicated unknown functions.

Entire domain basis functions can be generated using Tschebyscheff, Maclaurin, Legendre, Hermite polynomials, and sinusoidal, or other convenient functions.

### 2.6.2 Weighting (Testing) Functions

To improve the point-matching solution, an inner product $\langle w, g \rangle$ can be defined which is a scalar operation satisfying the laws of

$$\langle w, g \rangle = \langle g, w \rangle \tag{2.52a}$$

$$\langle bf + cg, w \rangle = b\langle f, w \rangle + c\langle g, w \rangle \tag{2.52b}$$

$$\langle g^*, g \rangle > 0 \qquad \text{if } g \neq 0 \tag{2.52c}$$

$$\langle g^*, g \rangle = 0 \qquad \text{if } g = 0 \tag{2.52d}$$

where $b$ and $c$ are scalars and the asterisk (*) indicates complex conjugation. A typical, but not unique, inner product is

$$\langle \mathbf{w}, \mathbf{g} \rangle = \iint_S \mathbf{w}^* \cdot \mathbf{g} ds \tag{2.53}$$

where the $w$'s are the *weighting* functions and $S$ is the surface of the structure being analyzed. Note that the functions $w$ and $g$ can be vectors.

The collocation (point-matching) method is a numerical technique whose solutions satisfy the electromagnetic boundary conditions only at discrete points. Between these points the boundary conditions may not be satisfied, and we define the deviation as a *residual* (e.g., residual $= \Delta E|_{\tan} = E(\text{scattered})|_{\tan} + E(\text{incident})|_{\tan} \neq 0$ on the surface of an electric conductor). To minimize the residual in such a way that its overall average over the entire structure approaches zero, the method of *weighted residuals* is utilized in conjunction with the inner product of (2.53). This technique, referred to as the *Moment Method* (MoM), does not lead to a vanishing residual at every point on the surface of a conductor, but it forces the boundary conditions to be satisfied in an average sense over the entire surface.

To accomplish this, we define a set of $N$ weighting functions $\{w_m\} = w_1, w_2, ..., w_N$ in the domain of the operator $F$. Forming the inner product between each of these functions, (2.47) results in

$$\sum_{n=1}^{N} a_n \langle w_m, F(g_n) \rangle = \langle w_m, h \rangle \qquad m = 1, 2, ..., N \tag{2.54}$$

This set of $N$ equations may be written in matrix form as

$$[F_{mn}][a_n] = [h_m] \tag{2.55}$$

where

$$[F_{mn}] = \begin{bmatrix} \langle w_1, F(g_1)\rangle & \langle w_1, F(g_2)\rangle & \cdots & \langle w_1, F(g_N)\rangle \\ \langle w_2, F(g_1)\rangle & \langle w_2, F(g_2)\rangle & \cdots & \langle w_2, F(g_N)\rangle \\ \vdots & \vdots & \ddots & \vdots \\ \langle w_N, F(g_1)\rangle & \langle w_N, F(g_2)\rangle & \cdots & \langle w_N, F(g_N)\rangle \end{bmatrix} \tag{2.55a}$$

$$[a_n] = \begin{bmatrix} a_1 \\ a_2 \\ \vdots \\ a_N \end{bmatrix} \qquad [h_m] = \begin{bmatrix} \langle w_1, h\rangle \\ \langle w_2, h\rangle \\ \vdots \\ \langle w_N, h\rangle \end{bmatrix} \tag{2.55b}$$

The matrix of (2.55) may be solved for the $a_n$ by inversion, and it can be written as

$$[a_n] = [F_{mn}]^{-1}[h_m] \tag{2.56}$$

The choice of weighting functions is important in that the elements of $\{w_m\}$ must be linearly independent, so that the $N$ equations in (2.54) will be linearly independent. Further, it will generally be advantageous to choose weighting functions that minimize the computations required to evaluate the inner product. A particular choice of functions may be to let the weighting and basis function be the same, that is, $w_n = g_n$. More generally, $w_n = g_n^*$ when $g_n$ is complex. This technique is known as *Galerkin's method.*

### 2.6.3 Numerical Electromagnetic Code (NEC)

The Numerical Electromagnetic Code (NEC) is a user-oriented FORTRAN program developed at Lawrence Livermore National Laboratory. It is a MoM code for analyzing the interaction of electromagnetic waves with arbitrary structures consisting of conducting wires and surface-patches. It combines an integral equation for smooth surfaces with one for wires to provide convenient and accurate modeling for a wide

range of applications. The code can model antennas, scatterers, as well as nonradiating networks and transmission lines, perfect and imperfect conductors, lumped element loading, and perfect and imperfect conducting ground planes.

It uses the EFIE for thin wires and the MFIE for surfaces. The EFIE used is Pocklinton's equation (2.37) for perfectly conducting wires. Finite conductivity is treated by impedance loading. The current expansion function (basis function) used for wires is, for the $j$th segment,

$$I_j(z) = A_j + B_j \sin[k(z - z_j)] + C_j \cos[k(z - z_j)] \tag{2.57}$$

where $z_j$ is the center of the $j$th wire segment. So the basis function is a three-term function (constant, sine and cosine) for wires. For surfaces, patches are used as the basic element and these are specified by their center point, area and normal. The current is assumed to be a constant over each patch, with components in two mutually orthogonal directions. Wires can only be attached to patches at their centers. For both wires and patches, the weighting function used in NEC is delta function, which necessarily gives an unsymmetrical impedance matrix.

The excitation in NEC can be either an applied voltage source or an incident plane wave. The program computes induced currents and charges, near- and far-zone electric and magnetic fields, radar cross section, impedances and admittances, gain and directivity, power budget, and antenna-to-antenna coupling.

## 2.7 Physical Optics Approximation (PO)

PO is perhaps the most flexible technique for RCS analysis of conductors. Due to the nature of the approximation, it works best for electrically large bodies, such as large flat surfaces. It is viable since it is the one of the fastest method devised so far for simple objects. The PO method uses the surface currents as obtained from Geometrical Optics (GO). These currents are integrated to get the scattered field.

### 2.7.1 Physical Equivalence Principle

The problem of Fig. 2.4a, scattering of $\mathbf{E}$ and $\mathbf{H}$ by a perfect electric conducting (PEC) obstacle, is of much practical concern. It can be formulated by the *physical equivalence principle.*

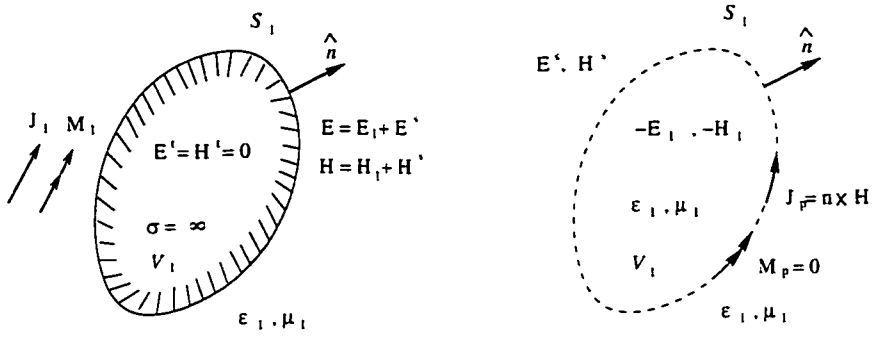


Figure 2.4: Physical equivalent for scattering by a perfect electric conducting (PEC) obstacle [1].

In the absence of the obstacle, the fields produced by $\mathbf{J}_1$ and $\mathbf{M}_1$ are $\mathbf{E}_i$ and $\mathbf{H}_i$, which we assume can be calculated or are given. In the presence of the obstacle (PEC in this case), the fields outside the obstacle are $\mathbf{E}$ and $\mathbf{H}$ and inside the obstacle are equal to zero. The fields $\mathbf{E}$ and $\mathbf{H}$ are related to $\mathbf{E}_i$ and $\mathbf{H}_i$ by

$$\mathbf{E} = \mathbf{E}_i + \mathbf{E}^s \tag{2.58a}$$

$$\mathbf{H} = \mathbf{H}_i + \mathbf{H}^s \tag{2.58b}$$

where $\mathbf{E}^s$ and $\mathbf{H}^s$ are *scattered fields* introduced by the obstacle.

According to the boundary condition, over the boundary $S_1$ of the conductor, the total tangential components of the $\mathbf{E}$ field are equal to zero and the total tangential components of the $\mathbf{H}$ field are equal to the induced current density $\mathbf{J}$. In equation

form, we have over $S_1$,

$$\mathbf{M} = -\hat{\mathbf{n}} \times (\mathbf{E} - \mathbf{E}^t) = -\hat{\mathbf{n}} \times \mathbf{E} = -\hat{\mathbf{n}} \times (\mathbf{E}_i + \mathbf{E}^s) = 0 \tag{2.59a}$$

$$\mathbf{J} = \hat{\mathbf{n}} \times (\mathbf{H} - \mathbf{H}^t) = \hat{\mathbf{n}} \times \mathbf{H} = \hat{\mathbf{n}} \times (\mathbf{H}_i + \mathbf{H}^s) \tag{2.59b}$$

or

$$-\hat{\mathbf{n}} \times \mathbf{E}_i = \hat{\mathbf{n}} \times \mathbf{E}^s \tag{2.60a}$$

$$\mathbf{J} = \hat{\mathbf{n}} \times \mathbf{H}_i + \hat{\mathbf{n}} \times \mathbf{H}^s \tag{2.60b}$$

Therefore, the equivalent to the problem of Fig. 2.4a, computation of $\mathbf{E}^s$ and $\mathbf{H}^s$ outside of $S_1$, is that of Fig. 2.4b. Remember that $\mathbf{E}_i$, $\mathbf{H}_i$ and $\mathbf{E}^s$, $\mathbf{H}^s$ are solutions to Maxwell's equations outside $V_1$, so in the equivalent problems we retain the same medium $\epsilon_1$, $\mu_1$ inside and outside $V_1$. The equivalent of Fig. 2.4b will give $\mathbf{E}^s$, $\mathbf{H}^s$ outside of $S_1$ and $\mathbf{E}_i$, $\mathbf{H}_i$ inside $S_1$ because

$$\mathbf{M} = -\hat{\mathbf{n}} \times \mathbf{E} = -\hat{\mathbf{n}} \times (\mathbf{E}^s + \mathbf{E}_i) = -\hat{\mathbf{n}} \times [\mathbf{E}^s - (-\mathbf{E}_i)] = 0 \tag{2.61a}$$

$$\mathbf{J} = \hat{\mathbf{n}} \times \mathbf{H} = \hat{\mathbf{n}} \times (\mathbf{H}^s + \mathbf{H}_i) = \hat{\mathbf{n}} \times [(\mathbf{H}^s - (-\mathbf{H}_i)] \tag{2.61b}$$

We call the problem of Fig. 2.4b the *physical equivalent.* It can be solved since we assume that $\mathbf{J}$ radiates in one medium ($\epsilon_1$, $\mu_1$ everywhere).

The physical equivalent is used to develop electric and magnetic field integral equations designated, respectively, as EFIE and MFIE. These integral equations are then solved for the unknown current density $\mathbf{J}$ by presenting it with a series of finite terms of known functions (referred to as basis functions) but with unknown amplitude coefficients. This then allows the reduction of the integral equation to a number of algebraic equations that are usually solved by use of either matrix or iterative techniques. To date, the most popular numerical technique in applied electromagnetics for solving these integral equations is the Moment Method (MoM) which was discussed in Section 2.6.

### 2.7.2 Physical Optics

If the conducting obstacle of Fig. 2.4a is an infinite, flat, perfect electric conductor (infinite ground plane), then the physical equivalent problem of Fig. 2.4b is that of Fig. 2.5 where the electric current $\mathbf{J}$ is equal to

$$\mathbf{J} = \hat{\mathbf{n}} \times \mathbf{H} = \hat{\mathbf{n}} \times (\mathbf{H}^s + \mathbf{H}_i) = 2\hat{\mathbf{n}} \times \mathbf{H}_i \tag{2.62}$$

since the tangential components of the scattered $\mathbf{H}^s$ field ($\mathbf{H}^s|_{tan}$) are in phase and equal in amplitude to the tangential components of the incident $\mathbf{H}_i$ field ($\mathbf{H}_i|_{tan}$). The equivalent of Fig. 2.5 is referred to as the *physical optics* (PO).

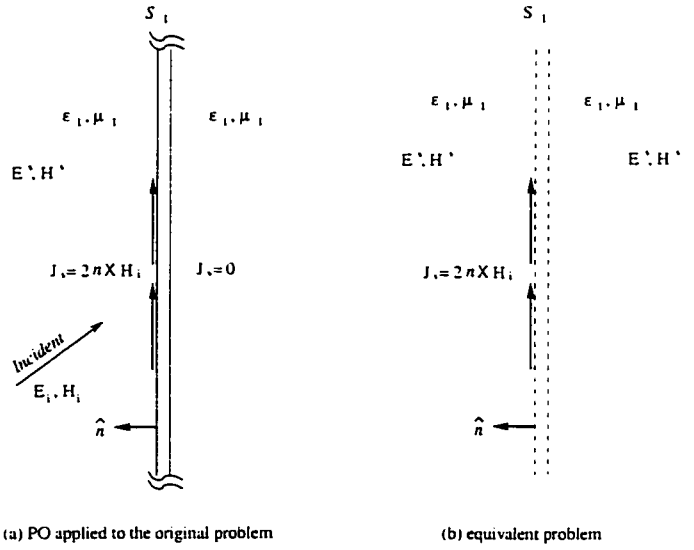


Figure 2.5: Physical Optics (PO) and the equivalence principle, applied to a PEC.

If we apply PO to any surface other than an infinite plane, the currents obtained from (2.62) are approximations of the MoM currents. PO is a popular approximation. It only approximates the surface current. How good the approximation is depends on the size, curvature, edges and wedges of the surface in relation to the wavelength, and the angle of the incident field. Generally, PO is only used for large, reasonably flat surfaces. However, it performs well for all surfaces of low curvature.

### 2.7.3 An Example

Supposing a uniform plane wave

$$\mathbf{E}^i = \hat{\boldsymbol{\theta}} E_0 e^{j\mathbf{k}\cdot\mathbf{r}} \tag{2.63}$$

is incident upon a flat rectangular plate of dimension $a = 2\ m$ and $b = 1\ m$, we want to find the scattered fields and RCS by using PO. Assume the incident field lies on the $xz$ plane ($\phi_i = 0^o$) and the wavelength $\lambda = 1\ m$.

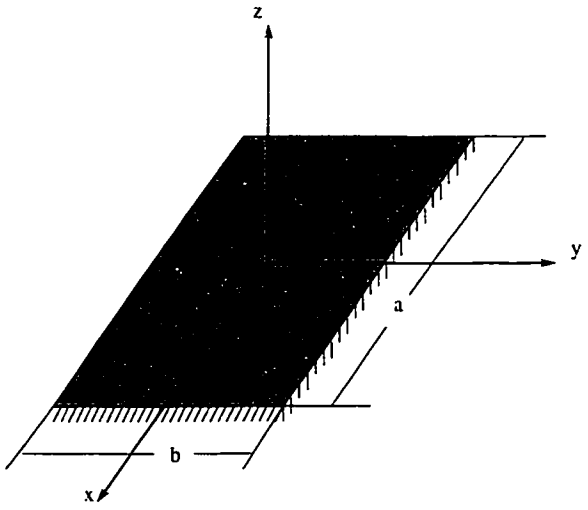


(a) Rectangular plate.

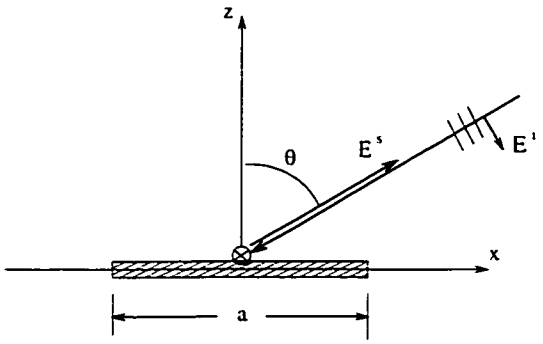


(b) The xz plane.

Figure 2.6: The geometry of uniform plane wave incident upon a rectangular plate in $xz$ plane.

The geometry of this task is shown in Fig. 2.6. Then the electric and magnetic field

components of the incident uniform plane wave can be written as

$$\mathbf{E}^i = \hat{\boldsymbol{\theta}} E_0 e^{j\mathbf{k}\cdot\mathbf{r}} = \hat{\boldsymbol{\theta}} E_0 e^{jk(x\sin\theta_i + z\cos\theta_i)} \tag{2.64}$$

$$\mathbf{H}^i = -\hat{\boldsymbol{\phi}} \frac{E_0}{\eta} e^{jk(x\sin\theta_i + z\cos\theta_i)} \tag{2.65}$$

At $z = 0$, the magnetic field reduces to

$$\mathbf{H}^i = -\hat{\boldsymbol{\phi}} \frac{E_0}{\eta} e^{jkx\sin\theta_i} = -\hat{\mathbf{y}} \frac{E_0}{\eta} e^{jkx\sin\theta_i} \tag{2.66}$$

Applying physical optics techniques, the current density induced on the plate can be approximated by

$$\mathbf{J}_s = 2\hat{\mathbf{n}} \times \mathbf{H}^i = 2\hat{\mathbf{z}} \times -\hat{\mathbf{y}} \frac{E_0}{\eta} e^{jkx'\sin\theta_i} = \hat{\mathbf{x}} \frac{2E_0}{\eta} e^{jkx'\sin\theta_i} \tag{2.67}$$

or

$$J_y = J_z = 0 \qquad \text{and} \qquad J_x = \frac{2E_0}{\eta} e^{jkx'\sin\theta_i} \tag{2.67a}$$

From (2.30), we have

$$\mathbf{A} = \frac{\mu}{4\pi} \int_S \mathbf{J}_s(x', y', z') \frac{e^{-jkR}}{R} ds' = \frac{\mu}{4\pi} \frac{e^{-jkr}}{r} \int_S \mathbf{J}_s e^{jk\hat{\mathbf{r}}\cdot\mathbf{r}'} ds' \tag{2.68}$$

where

$$\hat{\mathbf{r}} = \hat{\mathbf{x}}\sin\theta_s\cos\phi_s + \hat{\mathbf{y}}\sin\theta_s\sin\phi_s + \hat{\mathbf{z}}\cos\theta_s \tag{2.68a}$$

$$\mathbf{r}' = x'\hat{\mathbf{x}} + y'\hat{\mathbf{y}} + z'\hat{\mathbf{z}} \tag{2.68b}$$

In $xz$ plane, $\phi_s = 0^o$, then $\hat{\mathbf{r}} = \hat{\mathbf{x}}\sin\theta_s + \hat{\mathbf{z}}\cos\theta_s$. Thus,

$$\hat{\mathbf{r}} \cdot \mathbf{r}' = x'\sin\theta_s + z'\cos\theta_s \tag{2.69}$$

and (2.68) can be written as

$$\mathbf{A} = \frac{\mu}{4\pi} \frac{e^{-jkr}}{r} \int_S \mathbf{J}_s e^{jk(x'\sin\theta_s + z'\cos\theta_s)} ds' \tag{2.70}$$

On the plate, $z' = 0$, $\mathbf{A}$ reduces to

$$\mathbf{A} = \frac{\mu}{4\pi}\frac{e^{-jkr}}{r}\int_S \mathbf{J}_s e^{jkx'\sin\theta_s} ds' \tag{2.71}$$

and its $x$ component is

$$\begin{aligned} A_x &= \frac{\mu}{4\pi}\frac{e^{-jkr}}{r}\int_S J_x e^{jkx'\sin\theta_s} ds' \\ &= \frac{\mu}{4\pi}\frac{e^{-jkr}}{r}\int_{y'=-b/2}^{b/2}\int_{x'=-a/2}^{a/2}\frac{2E_0}{\eta}e^{jkx'\sin\theta_i}e^{jkx'\sin\theta_s}dx'dy' \\ &= \frac{2b\mu E_0}{4\pi\eta}\frac{e^{-jkr}}{r}\int_{x'=-a/2}^{a/2} e^{jkx'(\sin\theta_i+\sin\theta_s)}dx' \\ &= \frac{ab\mu E_0}{2\pi\eta}\frac{e^{-jkr}}{r}\frac{\sin(X)}{X} \end{aligned} \tag{2.72}$$

where

$$X = \frac{ka}{2}(\sin\theta_i + \sin\theta_s) \tag{2.72a}$$

For the far-field region. $E_\theta \cong -j\omega A_\theta$. Because of

$$A_\theta = \mathbf{A}\cdot\hat{\boldsymbol{\theta}} = A_x\hat{\mathbf{x}}\cdot\hat{\boldsymbol{\theta}} = A_x\cos\theta_s \tag{2.73}$$

the scattered E-field is

$$\begin{aligned} E_\theta^s &= -j\omega\cos\theta_s\frac{ab\mu E_0}{2\pi\eta}\frac{e^{-jkr}}{r}\frac{\sin(X)}{X} \\ &= -j\frac{abE_0}{\lambda}\frac{e^{-jkr}}{r}\left[\cos\theta_s\frac{\sin(X)}{X}\right] \end{aligned} \tag{2.74}$$

and the RCS can be calculated by

$$\begin{aligned} \sigma_{3-D} &= \lim_{r\to\infty}\left[4\pi r^2\frac{|E_\theta^s|^2}{|E_\theta^i|^2}\right] \\ &= 4\pi\left(\frac{ab}{\lambda}\right)^2\cos^2\theta_s\left[\frac{\sin(X)}{X}\right]^2 \end{aligned} \tag{2.75}$$

where $X$ is given by (2.72a).

In the case of computing the monostatic RCS, $\theta_i = \theta_s$. Thus

$$X = \frac{ka}{2}(\sin\theta_i + \sin\theta_s) \;=\; ka\sin\theta_i \tag{2.76}$$

then the scattered E-field reduces to

$$E_\theta^s \mid_{mono} = -j\frac{abE_0}{\lambda}\frac{e^{-jkr}}{r}\left[\cos\theta_i \frac{\sin(ka\sin\theta_i)}{ka\sin\theta_i}\right] \tag{2.77}$$

and the RCS is

$$\sigma_{3-D} \mid_{mono} = 4\pi\left(\frac{ab}{\lambda}\right)^2 \cos^2\theta_i \left[\frac{\sin(ka\sin\theta_i)}{ka\sin\theta_i}\right]^2 \tag{2.78}$$

Using a FORTRAN program *plate_rcs.f90*, which is listed in Appendix A.1, we can get the monostatic RCS of a $2\lambda$ by $1\lambda$ plate as shown in Fig. 2.7.

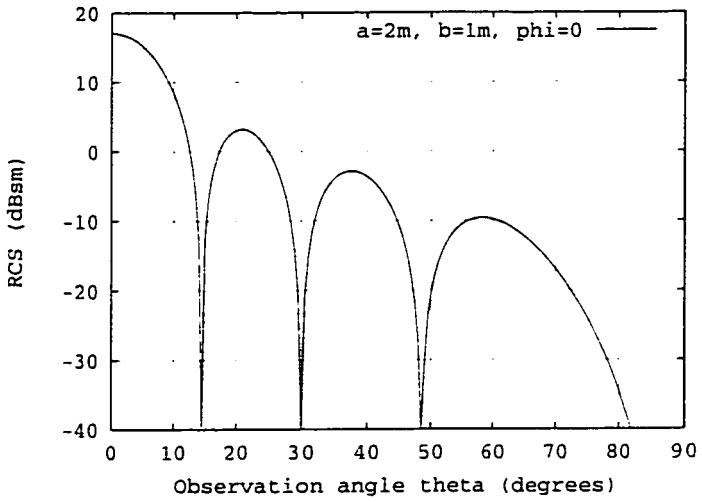


Figure 2.7: Monostatic RCS $\sigma_{\theta\theta}(\theta)$. PO solution for a $2m$ by $1m$ plate. The incident angle is $\phi = 0^o$ and $\lambda = 1m$.

# Chapter 3

# Some 3D Scattering Results from MoM and PO

In this chapter, we give the PO solutions for thin wires, plates, and a wire/plate combination. This is compared with the results from NEC-2, which is a MoM code for analyzing the interaction of electromagnetic waves with arbitrary structures consisting of conducting wires and surface-patches. Thus, we developed several NEC-2 and PO models.

We also studied the effect of holes in a plate, using PO and NEC-2. Finally, some interesting effects were observed by looking at a small vertical strip on the plate, which forms a dihedral reflector. This was studied by using NEC-2.

## 3.1 A Thin Wire

The studies of wires' RCS has been undergoing for several decades. Analysis techniques fall into two classes, depending on whether the wires are thin or thick. For thin wires, the MoM is extremely accurate and reasonably efficient. One also can use MoM dealing with thick wires, but the wires must be modeled as cylinders by using either wire grids or patches.

PO is inapplicable to a thin wire; however it can be extended as the eigenfunction/PO method. The main idea is to use the eigenfunction solution (rather than GO) to obtain the surface current on an infinitely long cylinder. For plane wave incidence,

this can be done exactly by using eigenfunction solution, whether the wires are thin or thick. Then we assume that truncating the wire does not appreciably alter the current, and obtain the scattered field by using radiation integral.

### 3.1.1 Detailed Analysis

We begin with a long cylinder of radius $a$ and length $-l/2 \leq z \leq l/2$ as shown in Fig. 3.1. The incident electric field is a $\hat{\theta}$ polarized uniform plane wave, in the $x-z$ plane ($\phi_i = 0$). In this instance, the electric field can be expressed as

$$\begin{aligned} \mathbf{E}^i &= \hat{\boldsymbol{\theta}} E_0 e^{jk(x\sin\theta_i + z\cos\theta_i)} \\ &= E_0(\hat{\mathbf{x}}\cos\theta_i - \hat{\mathbf{z}}\sin\theta_i)e^{jk(x\sin\theta_i + z\cos\theta_i)} \end{aligned} \tag{3.1}$$

The corresponding magnetic field is

$$\mathbf{H}^i = -\hat{\boldsymbol{\phi}}\frac{E_0}{\eta}e^{jk(x\sin\theta_i + z\cos\theta_i)} \tag{3.2}$$

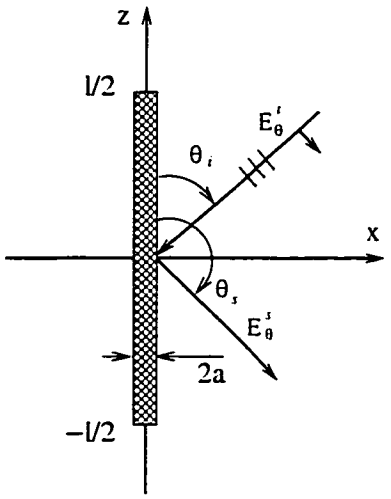


Figure 3.1: A $\hat{\boldsymbol{\theta}}$ polarized uniform plane wave incidents in the $x-z$ plane upon a circular cylinder of length $l$ and radius $a$.

Using the cylindrical wave transformations, the $z$ component of (3.1) can be expressed as

$$E_z^i = -E_0\sin\theta_i e^{jkz\cos\theta_i}\sum_{n=-\infty}^{\infty} j^n J_n(k\rho\sin\theta_i)e^{jn\phi} \tag{3.3}$$

From the eigenfunction solution, we can obtain the total magnetic field at the wire surface. Then, $\mathbf{J}_s = \hat{n} \times \mathbf{H}^t|_{\rho=a} = \hat{\rho} \times (\mathbf{H}^i + \mathbf{H}^s)|_{\rho=a}$ can be used to obtain the surface current. The current density induced on the surface of the wire can be expressed as

$$J_z = -\frac{2E_0}{\pi ka\eta \sin\theta_i} e^{jkz\cos\theta_i} \sum_{n=0}^{\infty} \frac{j^n \epsilon_n \cos(n\phi)}{H_n^{(2)}(ka\sin\theta_i)} \tag{3.4}$$

where $\epsilon_0 = 1$, $\epsilon_n = 2$ is Neumann's number. If the wire is thin, we can use just the leading term of the series, and the approximation is

$$H_0^{(2)}(x) \approx 1 - j\frac{2}{\pi}\ln(\frac{\gamma x}{2}) \tag{3.5}$$

where $\gamma = 1.781$. Then (3.4) reduces to

$$J_z = -\frac{jE_0 e^{jkz\cos\theta_i}}{a\omega\mu\sin\theta_i\{j\pi/2 + \ln[(\gamma ka/2)\sin\theta_i]\}} \tag{3.6}$$

From (3.6), we can see that the eigenfunction/PO solution for $J_z$ is a traveling wave. Actually, there should exist two components, $e^{jkz\cos\theta_i}$ and $e^{-jkz\cos\theta_i}$, but the first one is strong and the second one is weak.

From (2.43) and (2.32), we can use the radiation integral

$$\begin{aligned} A_z &= \frac{\mu}{4\pi}\int_{-l/2}^{l/2} I_z \frac{e^{-jkR}}{R} dz' \\ &= \frac{\mu}{4\pi}\frac{e^{-jkr}}{r}\int_{-l/2}^{l/2} 2\pi a J_z(z') e^{jk\hat{\mathbf{r}}\cdot\mathbf{r}'} dz' \end{aligned} \tag{3.7}$$

Because $\hat{\mathbf{r}} \cdot \mathbf{r}' = z'\cos\theta_s$ in our problem, $A_z$ reduces to

$$\begin{aligned} A_z &= \frac{\mu a}{2}\frac{e^{-jkr}}{r}\int_{-l/2}^{l/2} -\frac{jE_0 e^{jkz\cos\theta_i}}{a\omega\mu\sin\theta_i\{j\pi/2 + \ln[(\gamma ka/2)\sin\theta_i]\}} e^{jkz'\cos\theta_s} dz' \\ &= -j\frac{E_0}{2\omega\sin\theta_i}\frac{1}{j\pi/2 + \ln[(\gamma ka/2)\sin\theta_i]}\frac{e^{-jkr}}{r}\int_{-l/2}^{l/2} e^{jkz'(\cos\theta_i + \cos\theta_s)} dz' \\ &= -j\frac{E_0}{2\omega\sin\theta_i}\frac{1}{j\pi/2 + \ln[(\gamma ka/2)\sin\theta_i]}\frac{e^{-jkr}}{r}\frac{\sin(U)}{U} \end{aligned} \tag{3.8}$$

where

$$U = \frac{kl}{2}(\cos\theta_i + \cos\theta_s) \tag{3.8a}$$

With $E_\theta \cong -j\omega A_\theta$ for the far-field region and $A_\theta = -A_z \sin\theta_s$, the scattered E-field can be given by

$$E_\theta^s = \frac{E_0 l}{2} \frac{\sin\theta_s}{\sin\theta_i} \frac{1}{j\pi/2 + \ln[(\gamma ka/2)\sin\theta_i]} \frac{e^{-jkr}}{r} \frac{\sin(U)}{U} \tag{3.9}$$

and using (2.18), the RCS can be calculated by

$$\begin{aligned} \sigma_{3-D} &= \lim_{r\to\infty} \left[ 4\pi r^2 \frac{|E_\theta^s|^2}{|E_\theta^i|^2} \right] \\ &= \pi l^2 \frac{\sin^2\theta_s}{\sin^2\theta_i} \frac{1}{\pi^2/4 + \ln^2[(\gamma ka/2)\sin\theta_i]} \frac{\sin^2(U)}{U^2} \end{aligned} \tag{3.10}$$

### 3.1.2 Results

We computed the bistatic RCS for a thin wire with radius $a = 0.005\lambda$, length $l = 4\lambda$ and $\lambda = 1m$, as shown in Fig. 3.2. Comparison was made with the MoM code NEC-2. The numerical results in Fig. 3.2 for broadside incidence show very good agreement of eigenfunction/PO and NEC-2.

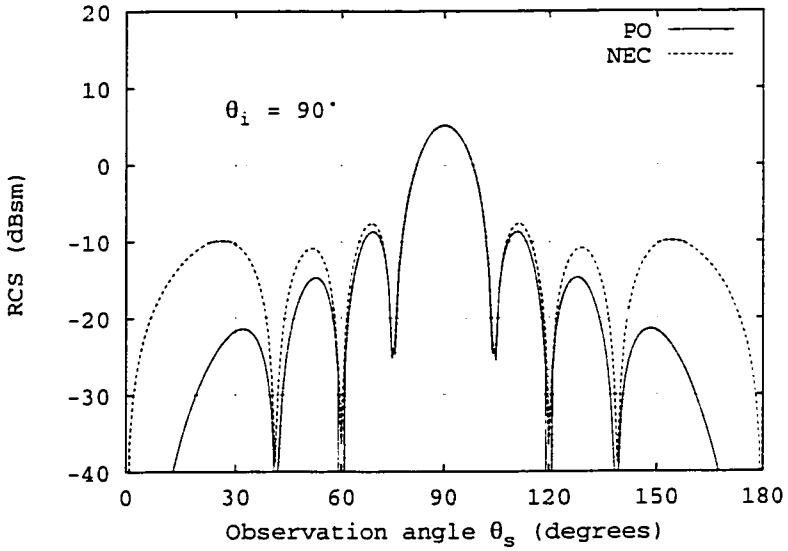


Figure 3.2: Bistatic RCS $\sigma_{\theta\theta}(\theta_s)$ for a thin wire with radius $0.005m$ and length $4m$. Comparison of eigenfunction/PO and NEC-2. The incident angle is $\theta_i = 90^o$ and $\lambda = 1m$. The observer is at $\theta_s$.

In general, for an incident angle $\theta_i$, the specular scattering occurs at $\theta_s = \pi - \theta_i$. This can be seen in Fig. 3.3 and Fig. 3.4. We also note that the results deteriorate

when the incident angle is close to grazing along the wire. This is because the PO current approaches zero.

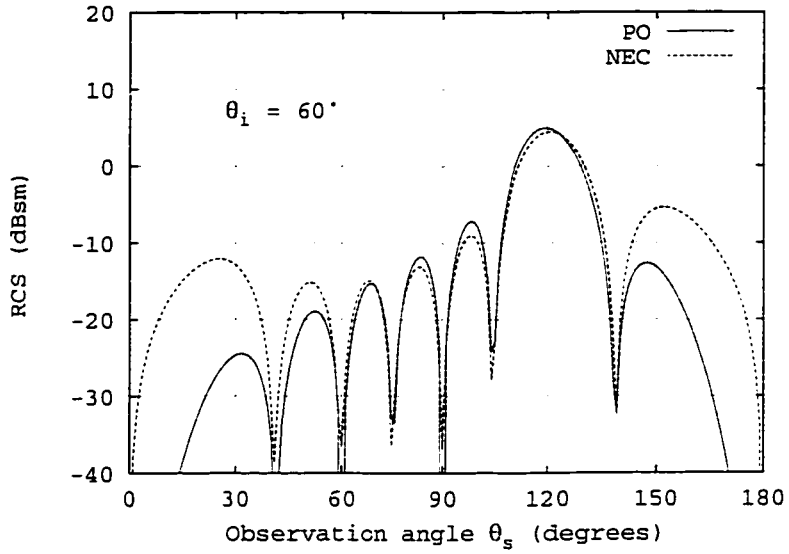


Figure 3.3: Bistatic RCS $\sigma_{\theta\theta}(\theta_s)$ for a thin wire with radius $0.005m$ and length $4m$. Comparison of eigenfunction/PO and NEC-2. The incident angle is $\theta_i = 60^o$ and $\lambda = 1m$. The observer is at $\theta_s$.

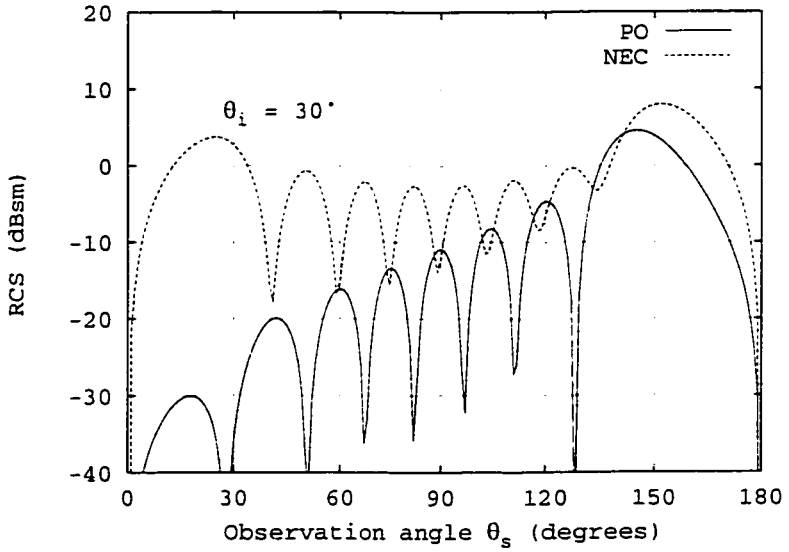


Figure 3.4: Bistatic RCS $\sigma_{\theta\theta}(\theta_s)$ for a thin wire with radius $0.005m$ and length $4m$. Comparison of eigenfunction/PO and NEC-2. The incident angle is $\theta_i = 30^o$ and $\lambda = 1m$. The observer is at $\theta_s$.

## 3.2 A Wire on the Plate

It is straightforward to obtain the scattered field of a wire/plate combination, using PO. The geometry of this problem is shown in Fig. 3.5, a $z$ directioned wire stands on a rectangular plate in $xy$ plane.

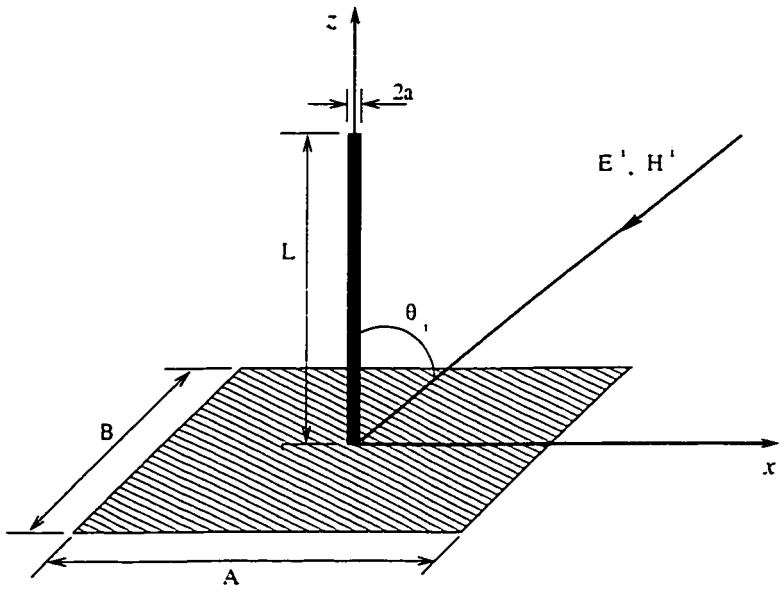


Figure 3.5: Geometry of a monopole illuminated by a uniform plane wave. The monopole has length $L$ and radius $a$.

Since the wire (monopole) is thin, its shadowing effects will be neglected. However, we must allow for the fact that the incident wave reflected from the plate will illuminate a portion of the wire. Hence, there are two incident waves (two scattered waves also) for the wire. They are shown in Fig. 3.6(a). Therefore, by adding these two wire fields and the field scattered by the plate, we can obtain the total scattered field.

Suppose the incident electric field is a $\hat{\theta}$ polarized uniform plane wave in the $xz$ plane ($\phi_i = 0$ or $180^o$). Then it can be expressed as

$$\mathbf{E}^i = \hat{\boldsymbol{\theta}} E_0 e^{jk(x\sin\theta_i\cos\phi_i + z\cos\theta_i)} \tag{3.11}$$

Using the same procedure as described in Section 2.7.3, we can obtain the PO

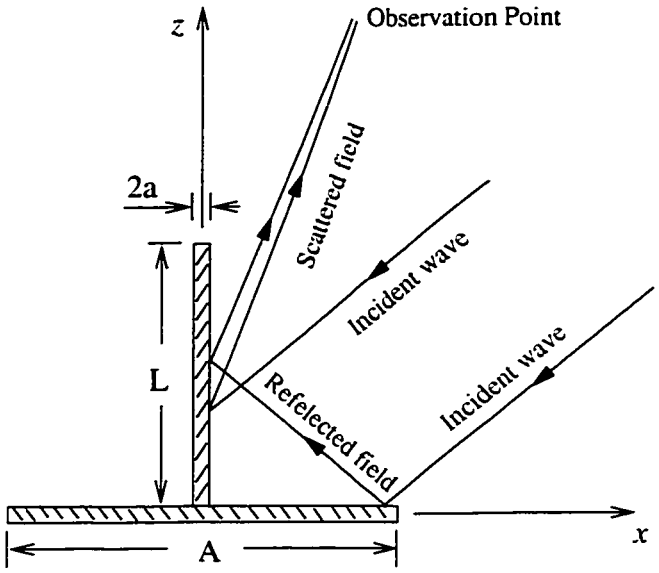


(a) The fields incidents upon the wire include direct incident wave and reflected wave from the plate

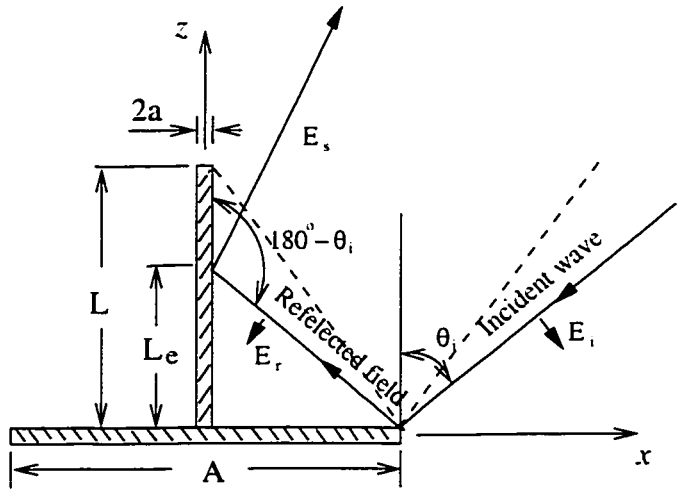


(b) The reflected field from the plate illuminate a portion of the wire

Figure 3.6: The fields on the wire when a monopole illuminated by a uniform plane wave. The monopole has length $L$ and radius $a$.

scattered field of the rectangular plate as

$$E_\theta^s \mid_{plate} = -j\frac{ABE_0}{\lambda}\frac{e^{-jkr}}{r}\left\{\cos\theta_s\cos(\phi_i-\phi_s)\left[\frac{\sin(X)}{X}\right]\right\} \tag{3.12}$$

where

$$X = \frac{kA}{2}(\sin\theta_i \cos\phi_i + \sin\theta_s \cos\phi_s) \tag{3.12a}$$

In the previous section, we had a solution for thin wire. So the first scattered field of the wire (caused by the direct incident wave) should be

$$E_\theta^s\,|_{wire_1} = \frac{E_0 L}{2}\frac{\sin\theta_s}{\sin\theta_i}\frac{1}{j\pi/2 + \ln[(\gamma ka/2)\sin\theta_i]}\frac{e^{-jkr}}{r}\frac{\sin(U)}{U} \tag{3.13}$$

where

$$U = \frac{kL}{2}(\cos\theta_i + \cos\theta_s) \tag{3.13a}$$

For the reflected field from the plate, from Fig. 3.6(b) we can find that it is still a $\hat{\theta}$ polarized uniform plane wave in the $xz$ plane ($\phi_i = 0$). But when the reflected field illuminates the wire, the incident angle becomes $180^0 - \theta$. We also noticed that if the incident angle is $\theta$ and the plate has a dimension of $A$ in $x$ direction, as shown in Fig. 3.6(b), then the equivalent wire length $L_{el}$ should be:

$$L_{el} = \left|\frac{A}{2\tan\theta_i}\right| \tag{3.14}$$

Thus, the second scattered field of the wire (caused by the reflected wave) can be expressed as

$$E_\theta^s\,|_{wire_2} = \frac{E_0 L_e}{2}\frac{\sin\theta_s}{\sin(\pi-\theta_i)}\frac{1}{j\pi/2 + \ln[(\gamma ka/2)\sin(\pi-\theta_i)]}\frac{e^{-jkr}}{r}\frac{\sin(U)}{U} \tag{3.15}$$

where

$$U = \frac{kL_e}{2}[\cos(\pi-\theta_i) + \cos\theta_s] \tag{3.15a}$$

$$L_e = \begin{cases} L_{el} & \text{if } L_{el} \le L. \\ L & \text{if } L_{el} > L. \end{cases} \tag{3.15b}$$

Then the total scattered field can be obtained by adding these three fields together

$$E_\theta^s\,|_{total} = E_\theta^s\,|_{plate} + E_\theta^s\,|_{wire_1} + E_\theta^s\,|_{wire_2} \tag{3.16}$$

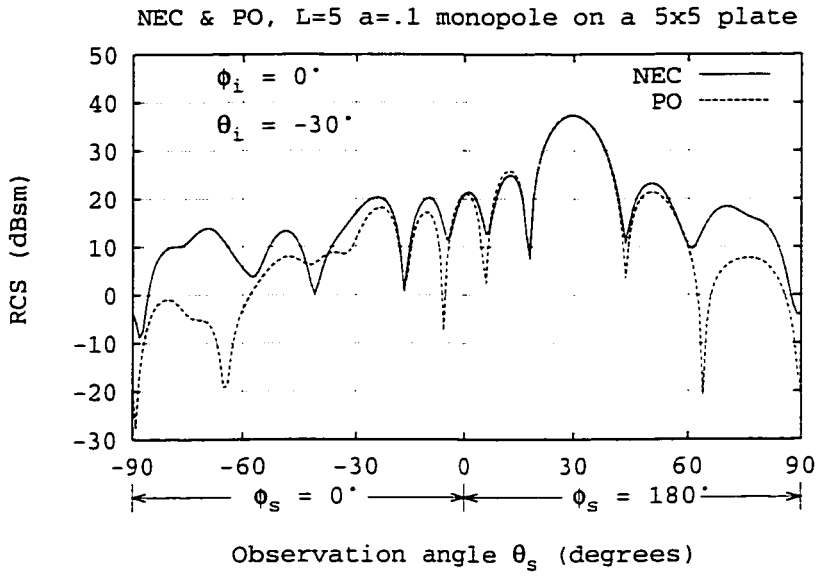


Figure 3.7: Bistatic RCS $\sigma_{\theta\theta}$ for a $l = 5\lambda$, $a = 0.1\lambda$ wire on a $5 \times 5$ rectangular plate. Comparison of PO and NEC. The incident angle is $\theta_i = -30^o$.

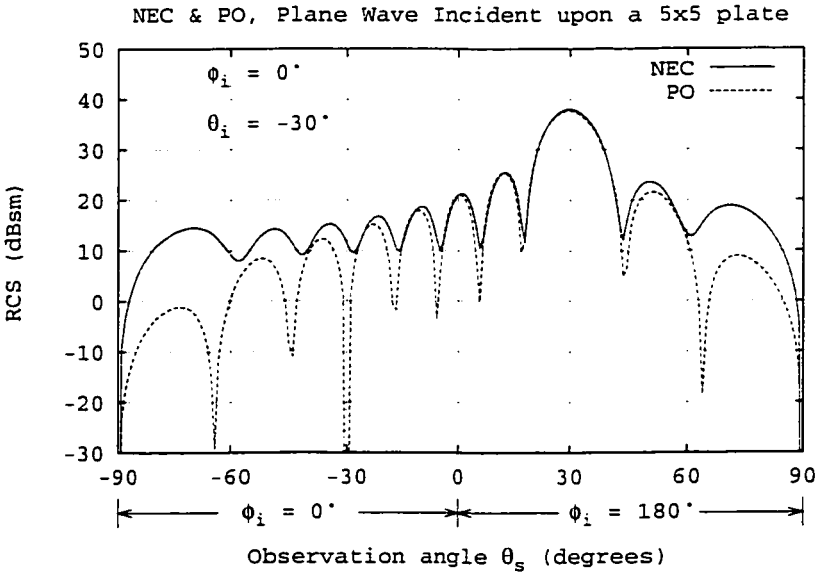


Figure 3.8: Bistatic RCS $\sigma_{\theta\theta}$ for a $5 \times 5$ rectangular plate without monopole. Comparison of PO and NEC. The incident angle is $\theta_i = -30^o$.

The FORTRAN program *plate_wire.f90*, which is listed in Appendix A.2, can be used to calculate the RCS for a wire/plate combination.

Fig. 3.7 shows the bistatic RCS for a $5\lambda$ by $5\lambda$ plate, with a wire of length $5\lambda$ and radius $0.1\lambda$ standing on it. NEC-2 was used for comparison with PO. In NEC-2, we modeled the plate by using wire grids. The distance between grids are $0.1\lambda$. Thus based on the same surface rule, the wire radius should be $0.1/2\pi = 0.0159\lambda$.

For comparison, the RCS for a plate without a wire on it are shown in Fig. 3.8. It is safe to assume the NEC-2 result is more accurate. We can see that the backscatter at $\theta = -30^o$ is affected by the presence of the wire. In the bistatic specular direction $\theta = 30^o$, it is obvious that the plate RCS dominates and the wire RCS is insignificant.

## 3.3 A Plate with Apertures

We developed NEC-2 and PO models for a large plate with holes. When a uniform plane wave is incident upon a rectangular plate with holes, we can get the RCS with different hole patterns by using NEC-2 and PO.

We still assume the incident electric field is a $\hat{\theta}$ polarized uniform plane wave in the $xz$ plane ($\phi_i = 0$ or $180^o$)

$$\mathbf{E}^i = \hat{\boldsymbol{\theta}} E_0 e^{jk(x\sin\theta_i\cos\phi_i + z\cos\theta_i)} \tag{3.17}$$

and the plate is in the $xy$ plane.

Suppose a rectangular plate is centered at $(x_0, y_0)$ with the dimensions as shown in Fig. 3.9. Then by using PO, we can obtain the scattered field as

$$E_\theta^s = -j\frac{abE_0}{\lambda}\frac{e^{-jkr}}{r}e^{jX_0}\left\{\cos\theta_s\cos(\phi_i - \phi_s)\left[\frac{\sin(X)}{X}\right]\right\} \tag{3.18}$$

where

$$X_0 = kx_0(\sin\theta_i\cos\phi_i + \sin\theta_s\cos\phi_s) \tag{3.18a}$$

$$X = \frac{ka}{2}(\sin\theta_i\cos\phi_i + \sin\theta_s\cos\phi_s) \tag{3.18b}$$

For comparison, we chose no hole, 1 hole, 5 holes and 13 holes on a $5\lambda$ by $5\lambda$ plate. We also let each hole to be a square with size $1\lambda$ by $1\lambda$, so we can use (3.18) to computer its scattered field. The hole patterns under examination are shown in Fig. 3.10.

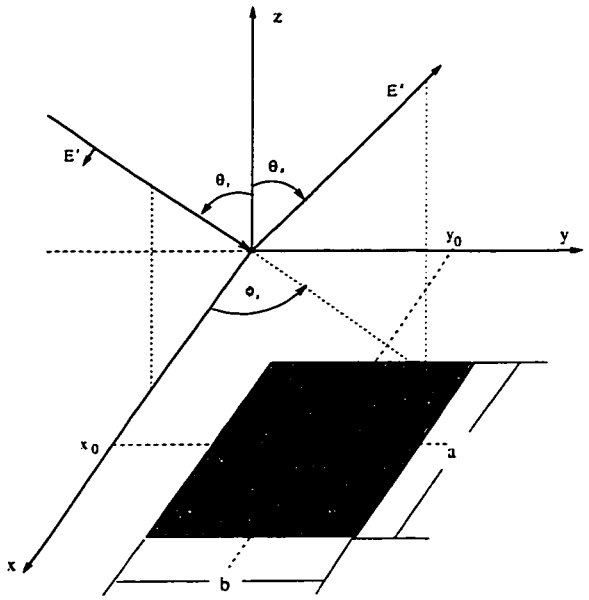


Figure 3.9: Uniform plane wave (in the $xz$ plane) incidents upon a $a$ by $b$ plate centered at $(x_0, y_0)$.

In order to solve the plate with apertures problem, first we should calculate the scattered fields of the plate using (3.18). Then, we calculate the scattered fields of each aperture. Finally, we can obtain the total scattered fields by subtracting each aperture fields from the plate fields. In equation form, it is

$$E_\theta^s \mid_{total} = E_\theta^s \mid_{plate} - \sum_{n=1}^{N} E_\theta^s \mid_{aperture_n} \tag{3.19}$$

For a uniform plane wave with an incident angle of 30 degrees, the bistatic RCS results are shown in Fig. 3.11. In Fig. 3.11 the figures on the left are obtained by using NEC-2, and those on the right are from PO.

From Fig. 3.11, we found that we needed a hole density of at least 50% to get any kind of significant effect. The hole and the plate have maximum RCS at the same bistatic angle. Hence, the hole RCS gets swamped out by the plate RCS, unless there are a lot of holes. The plate with many holes has the same phase relation between patches as a plate without holes, so the pattern is not greatly affected.

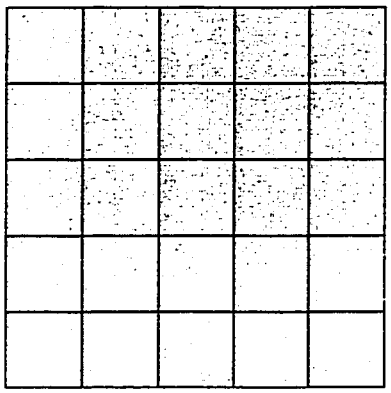

Pattern 1 (no hole)

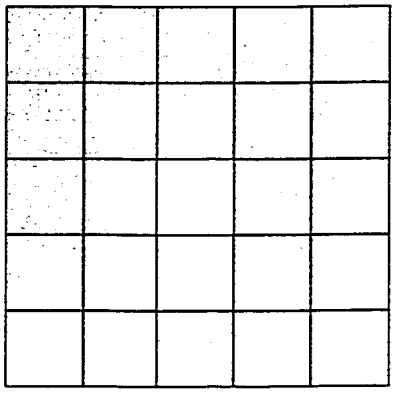

Pattern 2 (1 hole)

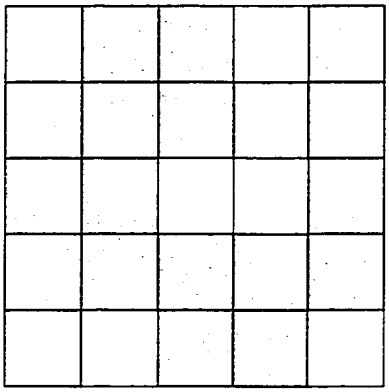

Pattern 3 (5 holes)

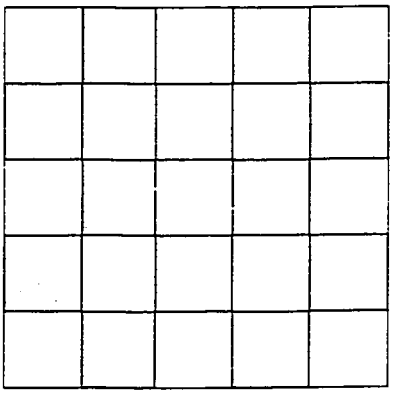

Pattern 4 (13 holes)

Figure 3.10: Four aperture patterns (no hole, 1 hole, 5 holes and 13 holes) on a $5\lambda \times 5\lambda$ square plate.

In fact, we can predict the RCS reduction at the specular direction by using a simplified RCS equation

$$RCS = \frac{4\pi A^2}{\lambda^2} \tag{3.20}$$

where $A$ is the area of the target. For instance, the area ratio between pattern 1 (no holes) and pattern 4 (13 holes) is 12/25, so the RCS reduction in dB should be $10\log(12/25)^2 = 6.4dB$. The plots in Fig. 3.11 proved this is true.

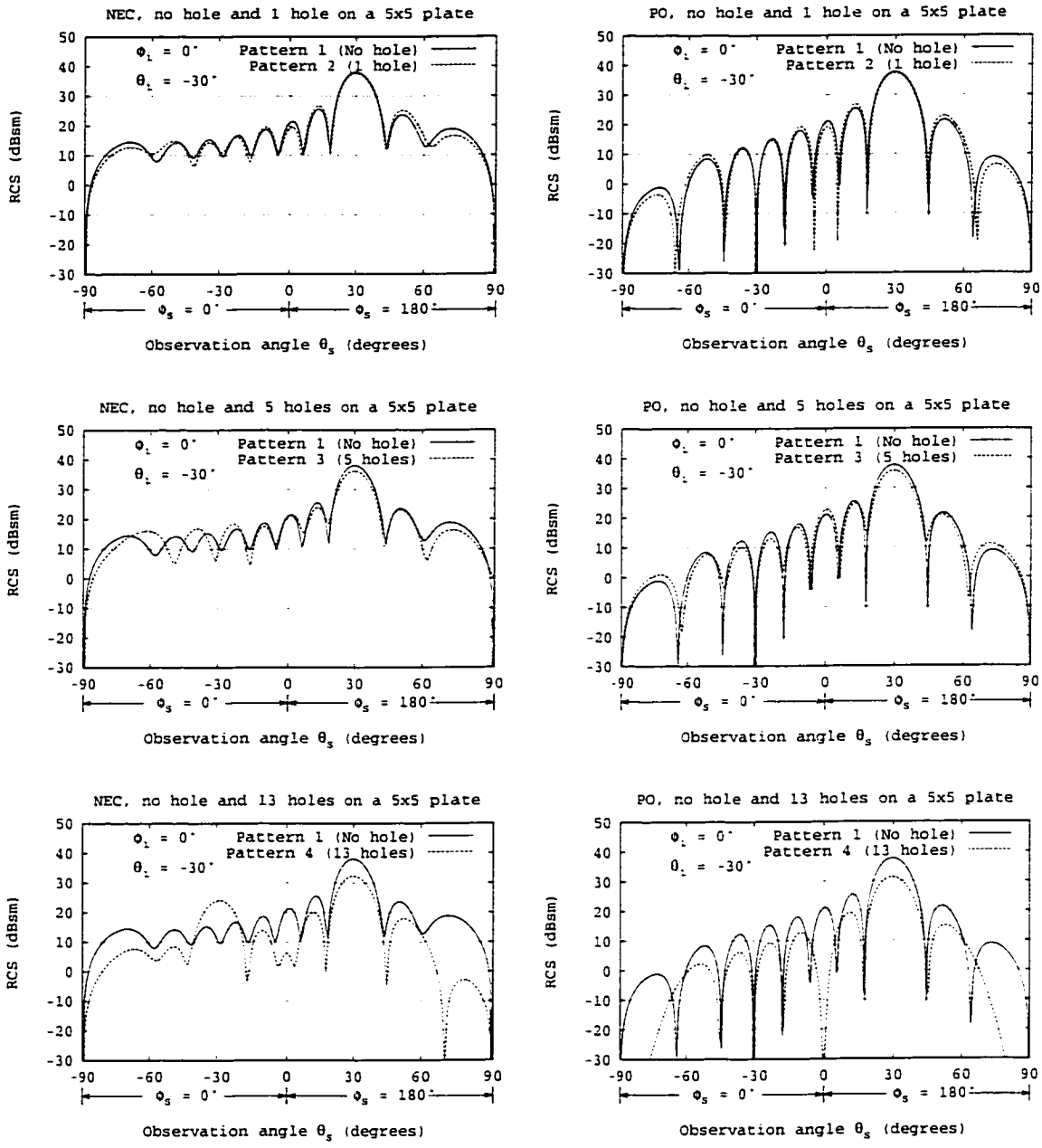


Figure 3.11: The comparison of bistatic RCS $\sigma_{\theta\theta}$ for different hole patterns when uniform plane wave incident upon a $5\lambda \times 5\lambda$ square plate with an incidence angle of 30 degrees. Comparison of PO and NEC.

## 3.4 A Vertical Strip on the Plate

We developed a NEC-2 model for a large plate with a small vertical strip. The geometry is shown in Fig. 3.12. We use the word "strip" to avoid confusion with the main plate. The main plate lies in the $xy$ plane, and the strip lies in the $yz$ plane.

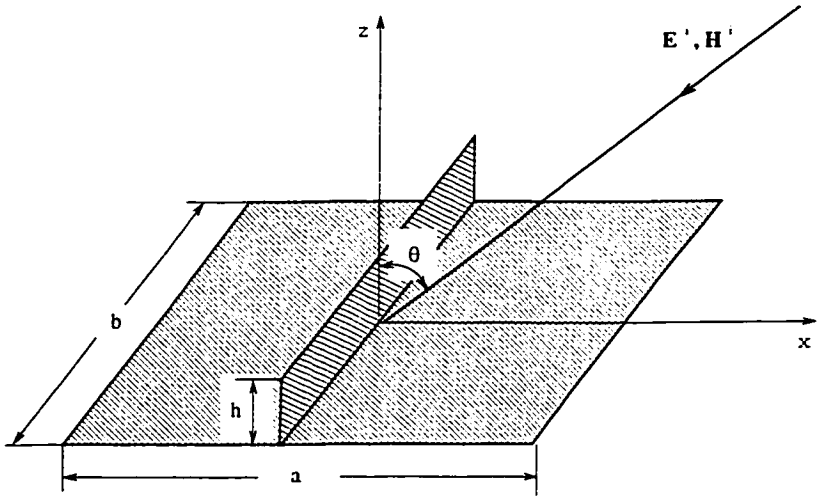


Figure 3.12: Geometry of rectangular plate with a vertical strip of height $h$, forming a dihedral reflector.

Again, we assume the incident electric field is a $\hat{\theta}$ polarized uniform plane wave in the $xz$ plane ($\phi_i = 0$ or $180^o$)

$$\mathbf{E}^i = \hat{\boldsymbol{\theta}} E_0 e^{jk(x \sin\theta_i \cos\phi_i + z\cos\theta_i)} \tag{3.21}$$

and we want to computer the co–polarized RCS.

Same as in previous sections, we still use a wire grid to model the plate and strip. The distance between grids is $0.1\lambda$, and so the wire radius equals to $0.0159\lambda$.

This structure forms a dihedral reflector. This corner reflector has a substantial effect, and it can be observed from the results because its RCS does not coincide with the large specular reflector of the main plate. Fig. 3.13 shows an interesting result. A strip of height $h = 1\lambda$ causes a strong RCS in the backscatter direction. The mono static RCS of this structure is shown in Fig. 3.14. We can see the great effect of the

strip in this structure when the incident (observation) angle is close to grazing of the plate.

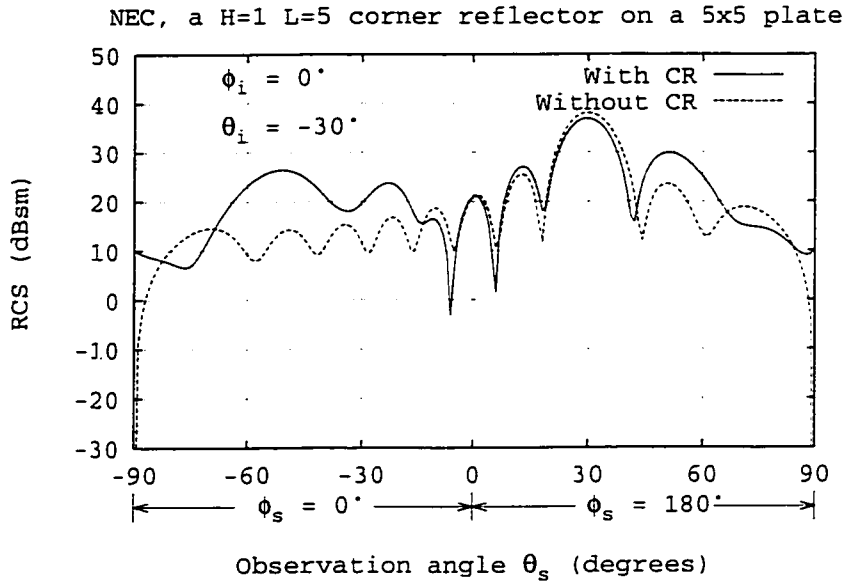


Figure 3.13: Bistatic RCS $\sigma_{\theta\theta}$ for a $5\lambda \times 5\lambda$ plate with and without a $1\lambda$ high, $5\lambda$ long corner reflector. The uniform plane wave incident at an angle of $\theta_i = 30^o$. NEC model

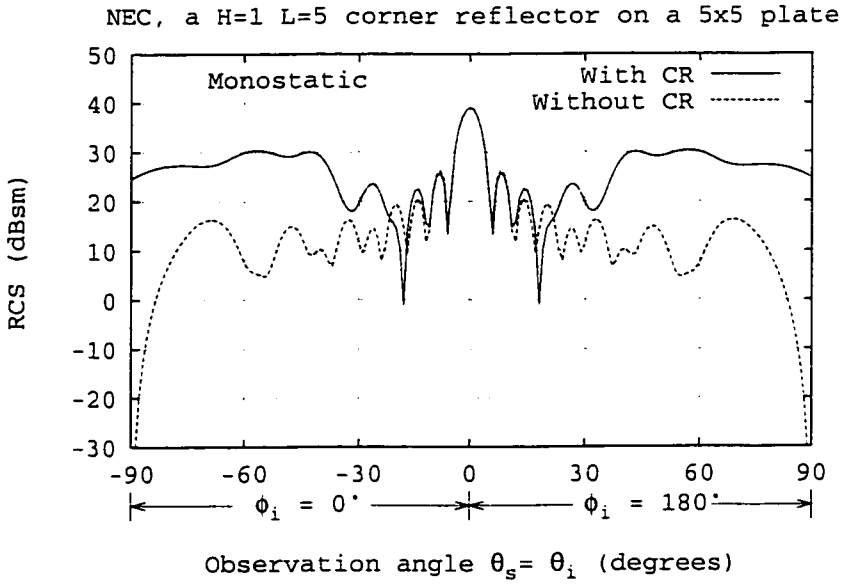


Figure 3.14: Monostatic RCS $\sigma_{\theta\theta}$ for a $5\lambda \times 5\lambda$ plate with and without a $1\lambda$ high, $5\lambda$ long corner reflector. NEC model

# Chapter 4

# 2D TM Scattering, PBPM and APE

In this chapter, first of all, we give the formulation of the methods of Pulse Basis Point Matching (PBPM), and Asymptotic Phasefront Extraction (APE). Then PBPM and APE were used to compute the surface current for a 2D strip, $TM_z$ case. Also, the RCS was obtained. Our purpose is to compare these two methods.

## 4.1 Formulation

Supposing a TM uniform plane wave is incident upon a finite width strip with incident angle $\phi_i$ as shown in Fig. 4.1, the incident field can be expressed as

$$E_z^i = e^{jk(x\cos\phi_i + y\sin\phi_i)} \tag{4.1}$$

and the current induced on the strip can be written as

$$J_z(x) = \sum_{n=1}^{N} a_n f_n(x) \tag{4.2}$$

From the incident electric field, we can write the scattered electric field at any observation point as

$$E_z^s = -\frac{k\eta}{4}\int_{x'=-w/2}^{w/2} H_0^{(2)}(kR) J_z(x')dx' \tag{4.3}$$

where

$$R = |r - r'| = \sqrt{(x-x')^2 + y^2} \tag{4.3a}$$

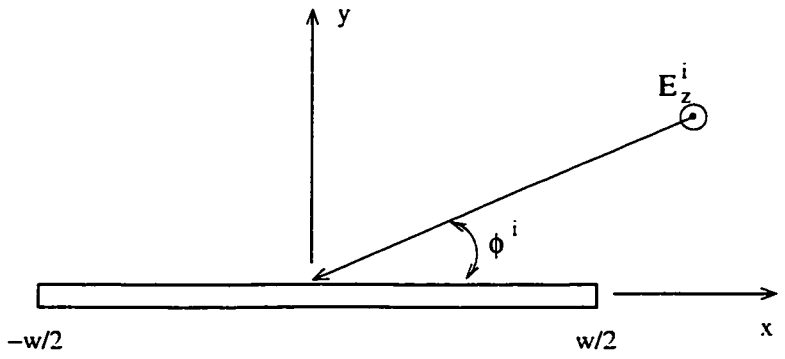


Figure 4.1: TM uniform plane wave incident on a strip.

By applying BC on the surface of the strip, we have

$$-E_z^i(x) \mid_{y=0} = E_z^s(x) \mid_{y=0} \tag{4.4}$$

Substituting (4.2) into (4.3), and applying (4.4) gives us

$$e^{jkx\cos\phi_i} = \frac{k\eta}{4}\sum_{n=1}^{N} a_n \int_{-w/2}^{w/2} H_0^{(2)}(k|x-x'|) f_n(x')dx' \tag{4.5}$$

or

$$E^i(x) = \sum_{n=1}^{N} a_n g_n(x) \tag{4.6}$$

where

$$E^i(x) = e^{jkx\cos\phi_i} \tag{4.6a}$$

$$g_n(x) = \frac{k\eta}{4}\int_{-w/2}^{w/2} H_0^{(2)}(k|x-x'|) f_n(x')dx' \tag{4.6b}$$

We need (4.5) to be true for all $x$ on the strip's surface.

We can use the MoM to solve (4.5). Multiplying both sides of (4.6) by weight function $w_m(x)$ and integrating over $-w/2 \le x \le w/2$ leads to following equation:

$$\int_{x=-w/2}^{w/2} E^i(x) w_m(x)dx = \int_{x=-w/2}^{w/2} \sum_{n=1}^{N} a_n g_n(x) w_m(x)dx \tag{4.7}$$

Note that (4.5) would need to be done as a single numerical integral, but (4.7) would have a double numerical integral. Putting (4.6a) and (4.6b) into (4.7) gives us

$$\int_{x=-w/2}^{w/2} e^{jkx\cos\phi_i} w_m(x)dx$$
$$= \sum_{n=1}^{N} a_n \int_{x=-w/2}^{w/2} \left[ \frac{k\eta}{4} \int_{x'=-w/2}^{w/2} H_0^{(2)}(k|x-x'|) f_n(x')dx' \right] w_m(x)dx \qquad (4.8)$$

or

$$V_m = \sum_{n=1}^{N} a_n Z_{mn} \qquad (4.9)$$

where

$$V_m = \int_{x=-w/2}^{w/2} e^{jkx\cos\phi_i} w_m(x)dx \qquad (4.9a)$$

$$Z_{mn} = \frac{k\eta}{4} \int_{x=-w/2}^{w/2} \int_{x'=-w/2}^{w/2} H_0^{(2)}(k|x-x'|) f_n(x') w_m(x)dx'dx \qquad (4.9b)$$

If we let $w_m(x) = f_m^*(x)$, then (4.9) becomes Galerkin's method.

### 4.1.1 Pulse Basis Point Matching (PBPM)

We can obtain the conventional PBPM solution by using pulses of width $\Delta$

$$f_n(x) = u(x - x_n + \Delta/2) - u(x - x_n - \Delta/2) \qquad (4.10)$$

where $u$ is the unit step function.

We want (4.5) to be true for all x on the strip. We cannot have this, but we can make it hold at $m$ points, i.e. we let

$$-E_z^i(x) \mid_{x=x_m} = E_z^s(x) \mid_{x=x_m} \qquad (4.11)$$

where $x = x_m$ is called a "match point", because the BC is met or "matched" at those points. Actually, by using "point matching", it is meant that the testing functions are

$$w_m(x) = \delta(x - x_m) \qquad (4.12)$$

Now, (4.5) can be rewritten as

$$e^{jkx_m \cos\phi_i} = \sum_{n=1}^{N} a_n \frac{k\eta}{4} \int_{\substack{n^{th} \\ pulse}} H_0^{(2)}(k|x_m - x'|)dx' \tag{4.13}$$

or

$$V_m = \sum_{n=1}^{N} a_n Z_{mn} \tag{4.14}$$

where

$$V_m = e^{jkx_m \cos\phi_i} \tag{4.14a}$$

$$Z_{mn} = \frac{k\eta}{4} \int_{\substack{n^{th} \\ pulse}} H_0^{(2)}(k|x_m - x'|)dx' \tag{4.14b}$$

Then, the main task is to evaluate the $Z_{mn}$.

For $m \neq n$, $Z_{mn}$ can be calculated by

$$Z_{mn} \cong \frac{k\eta}{4} H_0^{(2)}(k|x_m - x_n|) \int_{\substack{n^{th} \\ pulse}} dx' = \frac{k\eta}{4} H_0^{(2)}(k|x_m - x_n|)\Delta \tag{4.15}$$

For $m = n$, $Z_{mn}$ can be expressed as

$$Z_{nn} = \frac{k\eta}{4} \int_{-\frac{\Delta}{2}}^{\frac{\Delta}{2}} H_0^{(2)}(k|x'|)dx' = \frac{k\eta}{2} \int_0^{\frac{\Delta}{2}} H_0^{(2)}(kx')dx' \tag{4.16}$$

For small $x$, we have

$$H_0^{(2)}(x) \cong 1 - j\frac{2}{\pi} \ln(\frac{1.781x}{2}) \tag{4.17}$$

and (4.16) reduces to

$$\begin{aligned} Z_{nn} &= \frac{k\eta}{2} \int_0^{\frac{\Delta}{2}} \left[1 - j\frac{2}{\pi} \ln(\frac{1.781kx'}{2})\right] dx' \\ &= \frac{k\eta}{2} \left\{x' - j\frac{2}{\pi}x' \left[\ln(\frac{1.781kx'}{2}) - 1\right]\right\}_0^{\frac{\Delta}{2}} \end{aligned} \tag{4.18}$$

Note that

$$\lim_{x \to 0} x \ln(ax) = 0 \tag{4.19}$$

Thus, we have

$$Z_{nn} = \frac{k\eta}{2}\left\{\frac{\Delta}{2} - j\frac{2}{\pi}\frac{\Delta}{2}\left[\ln(\frac{1.781k\Delta}{4}) - 1\right]\right\}$$
$$= \frac{k\eta}{4}\left[1 - j\frac{2}{\pi}\ln(\frac{1.781k\Delta}{4e})\right]\Delta \tag{4.20}$$

After we obtain $V_m$ and $Z_{mn}$ and put them in (4.14), $a_n$ can be found by using the "Crout Method" to solve the system of linear equations. Then, by substituting (4.10) and $a_n$ to (4.2), we can obtain the PBPM current density on the strip.

According to the 2D $TM_z$ inhomogeneous wave equation solution, for a $z$ directed electric current $J_z$ at $\bar{\rho}' = \hat{\mathbf{x}}x' + \hat{\mathbf{y}}y'$, at an observation point $\bar{\rho} = \hat{\mathbf{x}}x + \hat{\mathbf{y}}y$, the magnetic vector potential $A_z$ can be expressed as

$$A_z = \int -j\frac{\mu J_z(\bar{\rho}')}{4}H_0^{(2)}(k|\bar{\rho} - \bar{\rho}'|)dl'$$
$$= -j\frac{\mu}{4}\int H_0^{(2)}(k|\bar{\rho} - \bar{\rho}'|)J_z(\bar{\rho}')dl' \tag{4.21}$$

Thus, by using the large argument approximation for the Hankel function

$$H_0^{(2)}(k\rho) \sim \sqrt{\frac{2}{\pi k\rho}}e^{-j(k\rho - \pi/4)} \tag{4.22}$$

the E-field produced by the electric current can be approximated by

$$E_z = -j\omega A_z = -\frac{\omega\mu}{4}\int H_0^{(2)}(k|\bar{\rho} - \bar{\rho}'|)J_z(\bar{\rho}')dl'$$
$$\sim -\eta\sqrt{\frac{jk}{8\pi}}\int \frac{e^{-jk|\bar{\rho}-\bar{\rho}'|}}{\sqrt{\bar{\rho}-\bar{\rho}'}}J_z(\bar{\rho}')dl'$$
$$\sim -\eta\sqrt{\frac{k}{8\pi}}e^{j\pi/4}\int \frac{e^{-jk|\bar{\rho}-\bar{\rho}'|}}{\sqrt{\bar{\rho}-\bar{\rho}'}}J_z(\bar{\rho}')dl' \tag{4.23}$$

In our problem, we have $|\bar{\rho} - \bar{\rho}'| \cong \rho - x'\cos\phi_s$ for the phase term and $|\bar{\rho} - \bar{\rho}'| \cong \rho$ for the distance term, and

$$J_z(\bar{\rho}') = \sum_{n=1}^{N} a_n f_n(x') \tag{4.24}$$

so the scattered field can be obtained from

$$E_z^s \cong -\eta\sqrt{\frac{k}{8\pi}}e^{j\pi/4}\frac{e^{-jk\rho}}{\sqrt{\rho}}\int_{-w/2}^{w/2} e^{jkx'\cos\phi_s}\sum_{n=1}^{N} a_n f_n(x')dx'$$

$$= -\eta\sqrt{\frac{k}{8\pi}}e^{j\pi/4}\frac{e^{-jk\rho}}{\sqrt{\rho}}\sum_{n=1}^{N} e^{jkx_n\cos\phi_s}a_n\Delta \tag{4.25}$$

where $x_n$ is the position of the n-th segment along the x axis, $a_n$ is the current density induced on the n-th segment, and $\Delta$ is the length of each segment. It is usually adequate to choose $0.1\lambda \leq \Delta \leq 0.2\lambda$.

### 4.1.2 Asymptotic Phasefront Extraction (APE)

The PBPM solution requires small segments. Following Kwon et al. [9], we can try including a phase taper in the basis functions. Thus, we replace (4.10) by

$$f_n(x) = [u(x - x_n + \Delta/2) - u(x - x_n - \Delta/2)]e^{jkx\cos\phi_i} \tag{4.26}$$

Using point matching, (4.5) becomes

$$e^{jkx_m\cos\phi_i} = \sum_{n=1}^{N} a_n\frac{k\eta}{4}\int_{\substack{n^{th}\\ pulse}} H_0^{(2)}(k|x_m - x'|)e^{jkx'\cos\phi_i}dx' \tag{4.27}$$

or

$$V_m = \sum_{n=1}^{N} a_n Z_{mn} \tag{4.28}$$

where

$$V_m = e^{jkx_m\cos\phi_i} \tag{4.28a}$$

$$Z_{mn} = \frac{k\eta}{4}\int_{\substack{n^{th}\\ pulse}} H_0^{(2)}(k|x_m - x'|)e^{jkx'\cos\phi_i}dx' \tag{4.28b}$$

For $m \neq n$, $Z_{mn}$ can be calculated by

$$Z_{mn} \cong \frac{k\eta}{4}H_0^{(2)}(k|x_m - x_n|)e^{jkx_n\cos\phi_i}\int_{\substack{n^{th}\\ pulse}} dx'$$

$$= \frac{k\eta}{4}H_0^{(2)}(k|x_m - x_n|)e^{jkx_n\cos\phi_i}\Delta \tag{4.29}$$

For $m = n$, $Z_{mn}$ can be expressed as

$$Z_{nn} = \frac{k\eta}{4}\left[1 - j\frac{2}{\pi}\ln(\frac{1.781k\Delta}{4e})\right] e^{jkx_n \cos\phi_i}\Delta \tag{4.30}$$

Note that $Z_{mn}$ is a symmetric array in PBPM, but here $Z_{mn}$ is an unsymmetric array.

Similar as in PBPM, from $V_m$ and $Z_{mn}$, we can obtain $a_n$. Then, by substituting (4.26) and $a_n$ to (4.2), we can obtain the APE current density on the strip. But now, we must divide each segment into small pieces and compute the current accounting to the phase taper.

By using (4.23) and (4.24), for the APE solution, the scattered field can be expressed as

$$\begin{aligned} E_z^s &\cong -\eta\sqrt{\frac{k}{8\pi}}e^{j\pi/4}\frac{e^{-jk\rho}}{\sqrt{\rho}}\int_{-w/2}^{w/2} e^{jkx'\cos\phi_s}\sum_{n=1}^{N} a_n f_n(x')dx' \\ &= -\eta\sqrt{\frac{k}{8\pi}}e^{j\pi/4}\frac{e^{-jk\rho}}{\sqrt{\rho}}\sum_{n=1}^{N} e^{j2kx_n\cos\phi_s} a_n\Delta \end{aligned} \tag{4.31}$$

### 4.1.3 Numerical Integration (NI)

From previous sections, we know that:

For PBPM

$$Z_{mn} = \frac{k\eta}{4}\int_{\substack{n^{th}\\ pulse}} H_0^{(2)}(k|x_m - x'|)dx' \tag{4.32}$$

Comparing it with (4.15) and (4.20), we can find that: when we compute $Z_{mn}$, we assume $H_0^{(2)}(k|x_m - x'|)$ is a constant inside the n-th segment, and it equals to $H_0^{(2)}(k|x_m - x_n|)$. Obviously, this would be true only when the segments length $\Delta$ is very small. If we use these equations for large $\Delta$, they will introduce significant errors on the surface current as well as RCS.

For large $\Delta$, we must use numerical integration to calculate $Z_{mn}$. Thus, we divide every segment to J pieces. If the sub-segment length is $\delta$, then we have $\Delta = J\delta$. So for PBPM

$$
\begin{aligned}
Z_{mn} &= \frac{k\eta}{4} \int_{\substack{n^{th} \\ pulse}} H_0^{(2)}(k|x_m - x'|)dx' \\
&= \frac{k\eta}{4} \int_{x_n-\Delta/2}^{x_n+\Delta/2} H_0^{(2)}(k|x_m - x'|)dx' \\
&= \frac{k\eta}{4} \sum_{i=1}^{J} H_0^{(2)}(k|x_m - x_i|)\delta \qquad (x_i = x_n - \Delta/2 + i\delta) \qquad (4.33)
\end{aligned}
$$

When we calculate $Z_{nn}$, if $|x_m - x_i| < \delta\lambda$, we note that the Hankel function is singular. We can use following equation to compute the values of Hankel function

$$
H_0^{(2)}(k|x_m - x_i|) \cong H_0^{(2)}(2\pi\delta) \cong 1 - j\frac{2}{\pi}\ln(1.781\pi\delta) \qquad (4.34)
$$

and obtain $Z_{nn}$.

For APE, we can use same procedure to implement NI.

## 4.2 Surface Current $J_s$

By using Pulse Basis Point Matching (PBPM) or Asymptotic Phasefront Extraction (APE) methods, we examined the surface current $J_s$ when a TM uniform plane wave is incident upon a strip. For a $2\lambda$ width strip illuminated by a plane wave at an angle of $\phi_i = 60^o$, we can get the magnitude and phase of the induced surface current density along the strip when $N = 8$ segments. The results are plotted in Fig. 4.2. It is important to note that each segment was divided into 100 slices when we calculate the APE current.

The plots in Fig. 4.2 show that the APE is highly suited to model the rapidly varying surface current phase. At the match points, the APE and the PBPM have good agreements. The phase slope in the APE is dictated by the incident plane wave. Hence the phase discontinuities seem inevitable. Nevertheless, the APE phase is closer to the expected physical behavior.

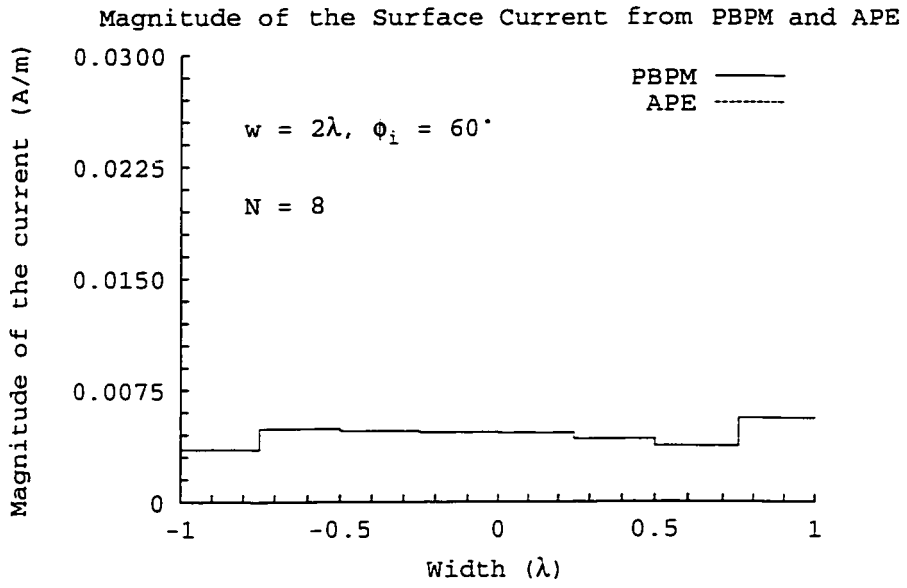


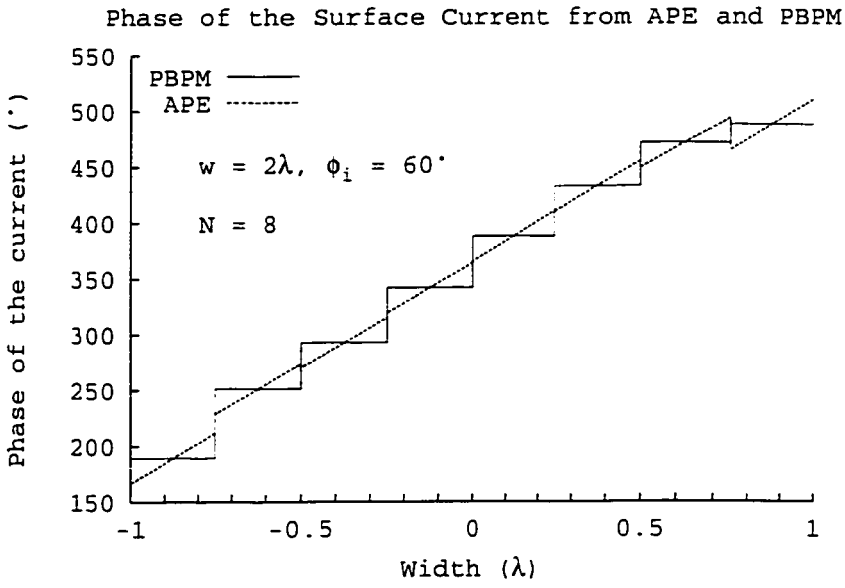


Figure 4.2: The surface current density along a strip of width $2\lambda$. $N = 8$. Comparison of PBPM and APE. TM uniform plane wave incident on the plate at an angle of $\phi_i = 60^o$.

We also computed the real part and imaginary part of the surface current of a $2\lambda$ width strip. After applying numerical integration, the comparisons of PBPM and APE are shown in Fig. 4.3.

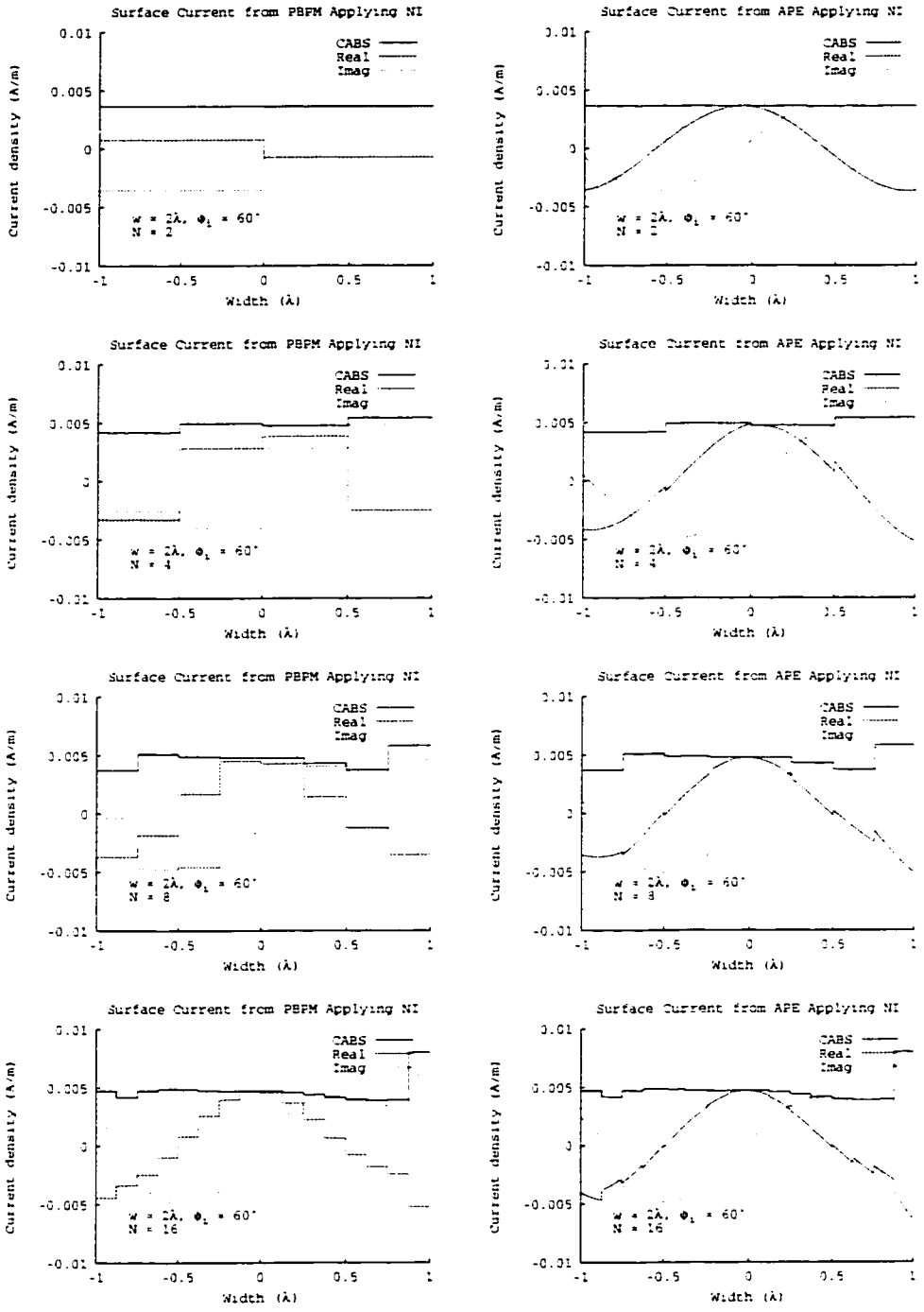


Figure 4.3: Real and imaginary parts of the surface current for different segment numbers $N$. Comparison of PBPM and APE applying NI with 100 steps per segment. TM uniform plane wave incident upon a $2\lambda$ width strip at an angle of $\phi_i = 60^o$.

For a $20\lambda$ width strip at the same condition, the surface current are shown in Fig. 4.4.

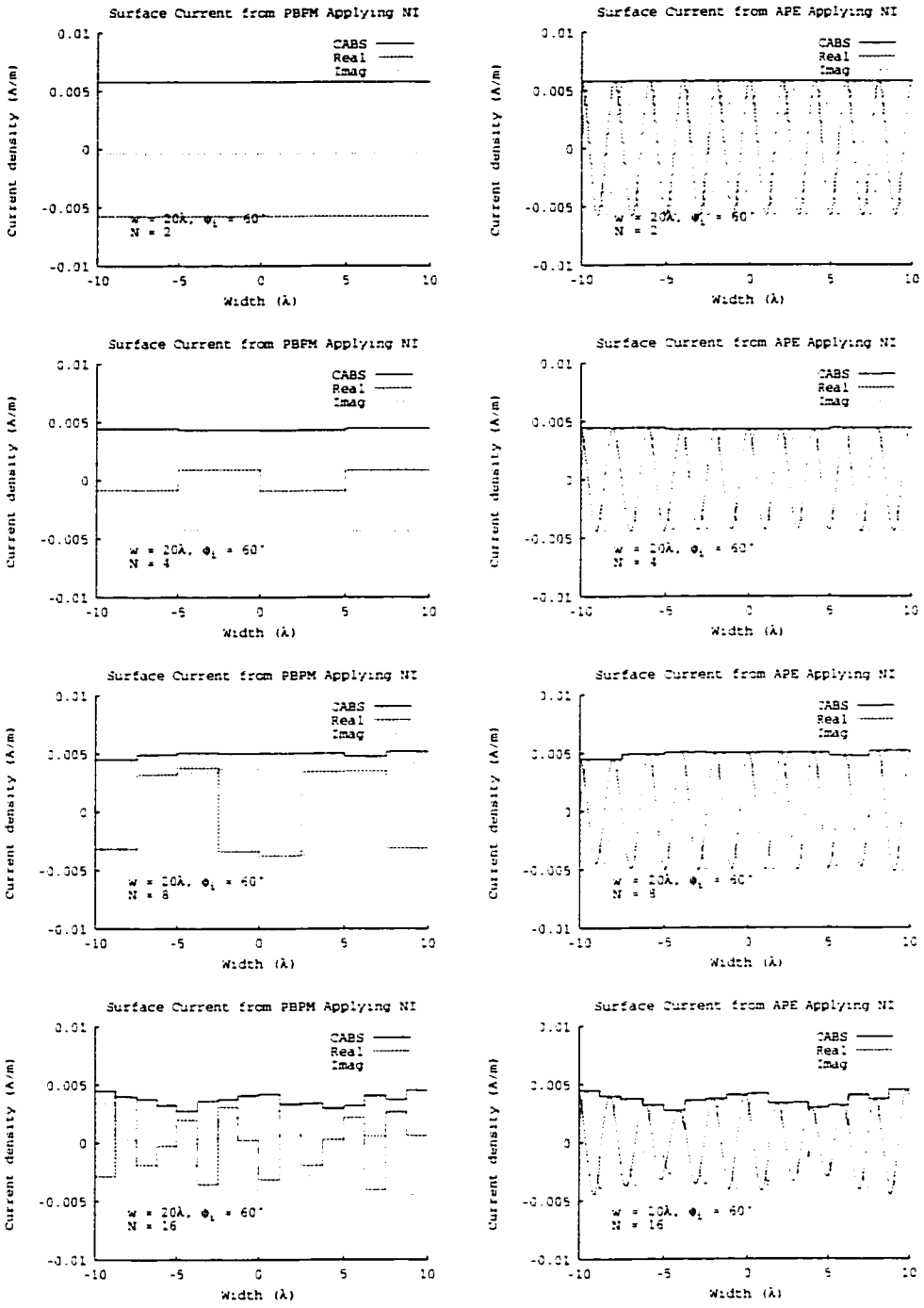


Figure 4.4: Real and imaginary parts of the surface current for different segment numbers $N$. Comparison of PBPM and APE applying NI with 100 steps per segment. TM uniform plane wave incident upon a $2\lambda$ width strip at an angle of $\phi_i = 60^o$.

## 4.3 RCS

From (4.25) and (4.31), we can calculate the scattered field of a finite width strip by applying Pulse Basis Point Matching (PBPM) or Asymptotic Phasefront Extraction (APE) methods. Then we can have the 2D scattering width (SW) by using (2.17).

### 4.3.1 $TM_z$ Plane Wave $60^o$ Incident

For a $2\lambda$ width strip, with a $TM_z$ plane wave incident at an angle of $60^o$, the results are plotted in Fig. 4.5. When we calculate APE current, we still divided each segments into 100 slices. In the plots, the PBPM with $N = 256$ is used as the benchmark solution.

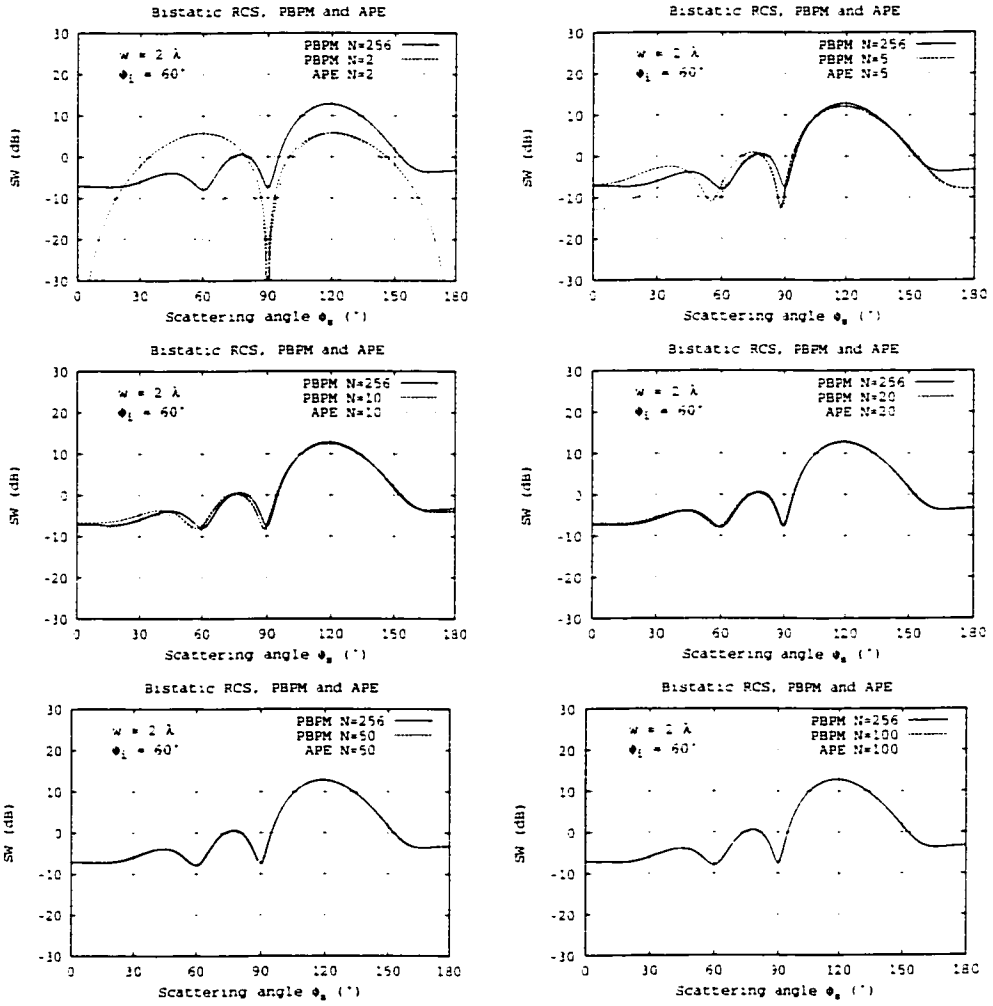


Figure 4.5: The bistatic RCS $\sigma_{\phi\phi}(\phi_s)$ of different segment numbers $N$. Comparison of PBPM and APE. TM uniform plane wave incident upon a $2\lambda$ width strip at an angle of $\phi_i = 60^o$.

Also, we can get the results for a $20\lambda$ width strip at the same condition. They are plotted in Fig. 4.6. Comparing with Fig. 4.5, we can make a conclusion: APE will give us better results for the objects with large dimensions.

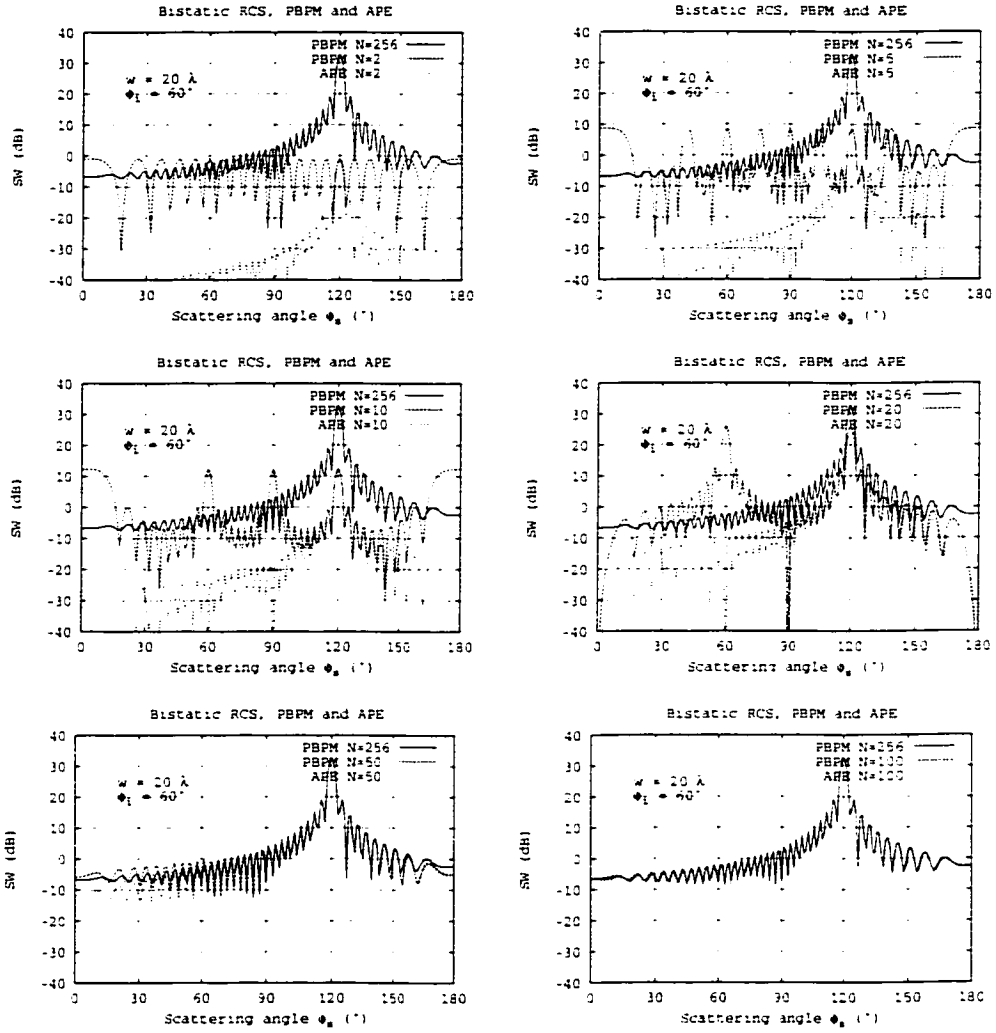


Figure 4.6: The bistatic RCS $\sigma_{\phi\phi}(\phi_s)$ of different segment numbers $N$. Comparison of PBPM and APE. TM uniform plane wave incident upon a $20\lambda$ width strip at an angle of $\phi_i = 60°$.

From Fig. 4.5 and Fig. 4.6, we can find that, at the specular point, the SW's at $N = 2$ are much lower than them at $N = 256$. The reason is that the magnitude of the current becomes smaller at $N = 2$ comparing to at $N = 256$. By applying numerical integration, we calculated the 2D scattering width (SW) for both $2\lambda$ and $20\lambda$ width

strips again. With a $TM_z$ plane wave incident at an angle of $60^o$, choosing the integral steps as 100 per segment, the results are plotted in Fig. 4.7 and Fig. 4.8. From these two figures, we confirmed that APE will give us better results for the objects with large dimensions.

Comparing Fig. 4.7 with Fig. 4.5 and Fig. 4.8 with Fig. 4.6, we can find the results in Fig. 4.7 and Fig. 4.8 are much better for large segments. So when the segments are large ($N$ is small), applying NI to RCS computation is very important.

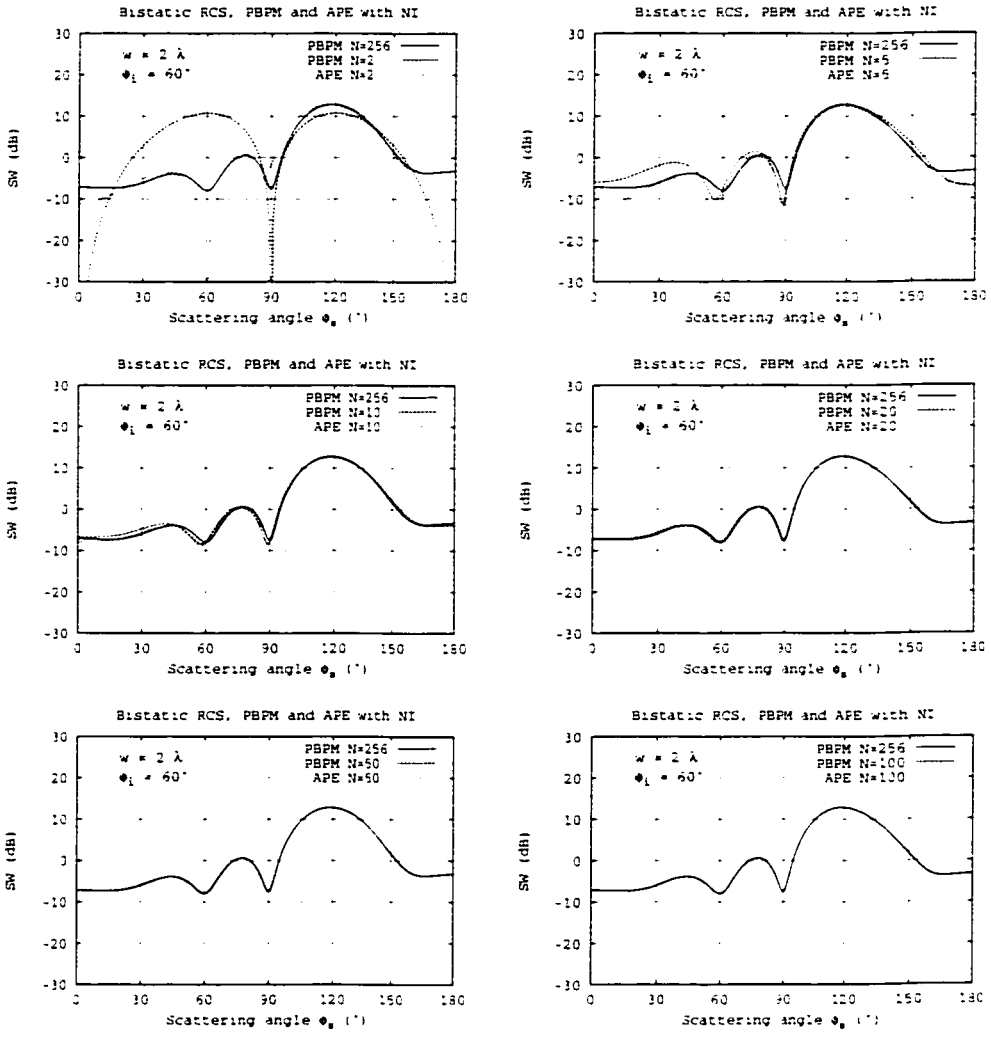


Figure 4.7: The bistatic RCS $\sigma_{\phi\phi}(\phi_s)$ of different segment numbers $N$. Comparison of PBPM and APE applying NI with 100 steps per segment. TM uniform plane wave incident upon a $2\lambda$ width strip at an angle of $\phi_i = 60^o$.

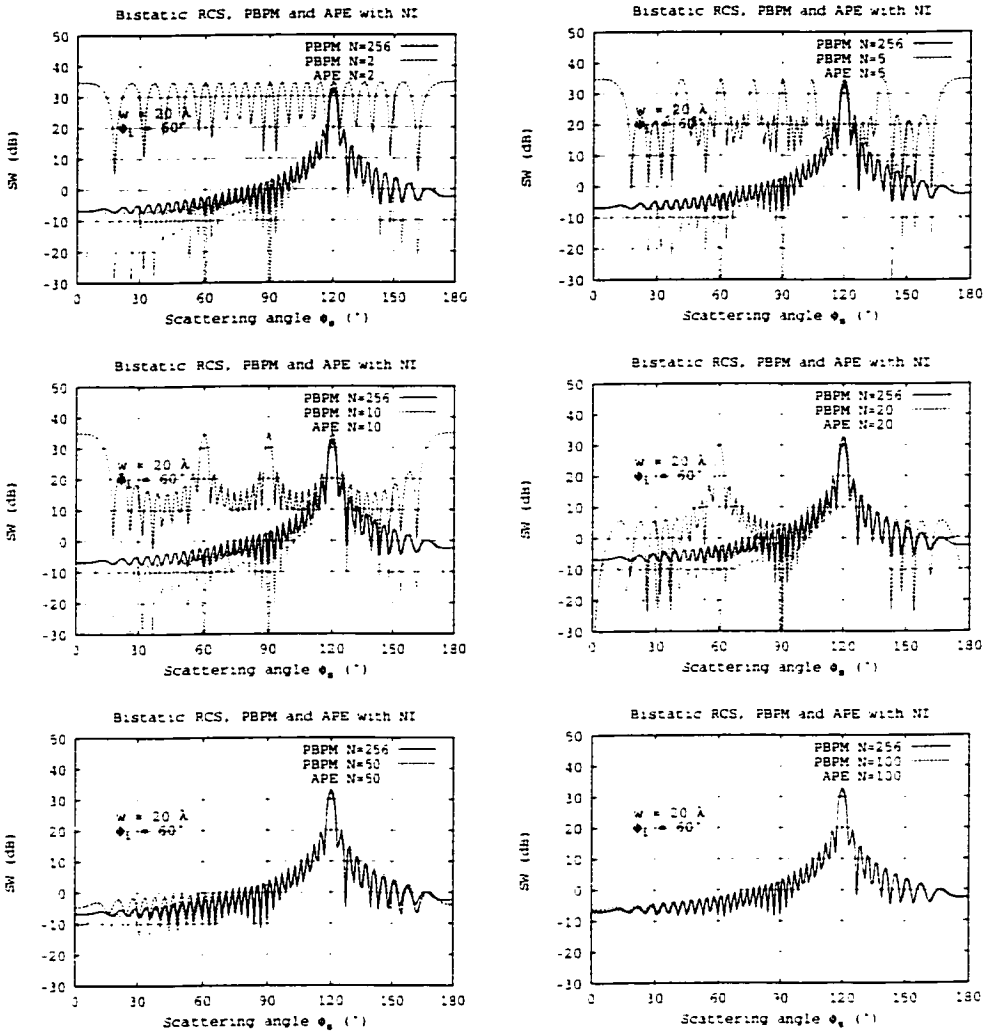


Figure 4.8: The bistatic RCS $\sigma_{\phi\phi}(\phi_s)$ of different segment numbers $N$. Comparison of PBPM and APE applying NI with 100 steps per segment. TM uniform plane wave incident upon a $20\lambda$ width strip at an angle of $\phi_i = 60^o$.

From Fig. 4.7 and Fig. 4.8, we can find that, PBPM can give us good SW results when segments length $\Delta \leq 0.2\lambda$ ($N = 10$ for $w = 2\lambda$ or $N = 100$ for $w = 20\lambda$). But for APE, even when $\Delta = 10\lambda$, the SW result still looks good.

Now, we increase the strip width to $200\lambda$. With a $TM_z$ plane wave incident at an angle of $60^o$, the SW results are plotted below. We can see APE can give us good SW results even when segments length $\Delta \leq 40\lambda$ ($N = 5$ for $w = 200\lambda$).

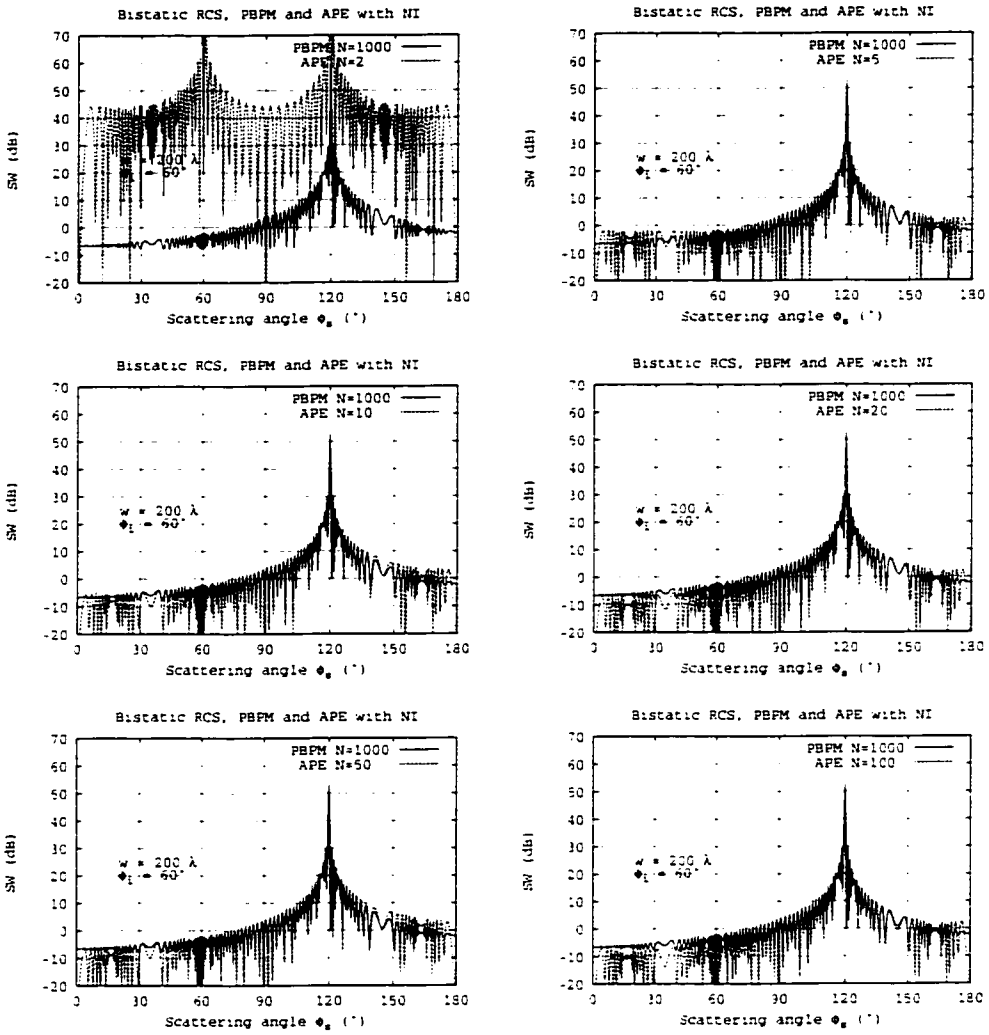


Figure 4.9: The bistatic RCS $\sigma_{\phi\phi}(\phi_s)$ of different segment numbers $N$. Comparison of PBPM and APE applying NI with 100 steps per segment. TM uniform plane wave incident upon a $200\lambda$ width strip at an angle of $\phi_i = 60^o$.

### 4.3.2 $TM_z$ Plane Wave Grazing Incident

One interesting question is that: does APE help RCS computation when a $TM_z$ plane wave is grazing incident on a strip ($\phi_i = 0$). For a $2\lambda$ width strip, by applying NI, the results are plotted in Fig. 4.10. We still use the PBPM with $N = 256$ as the benchmark solution.

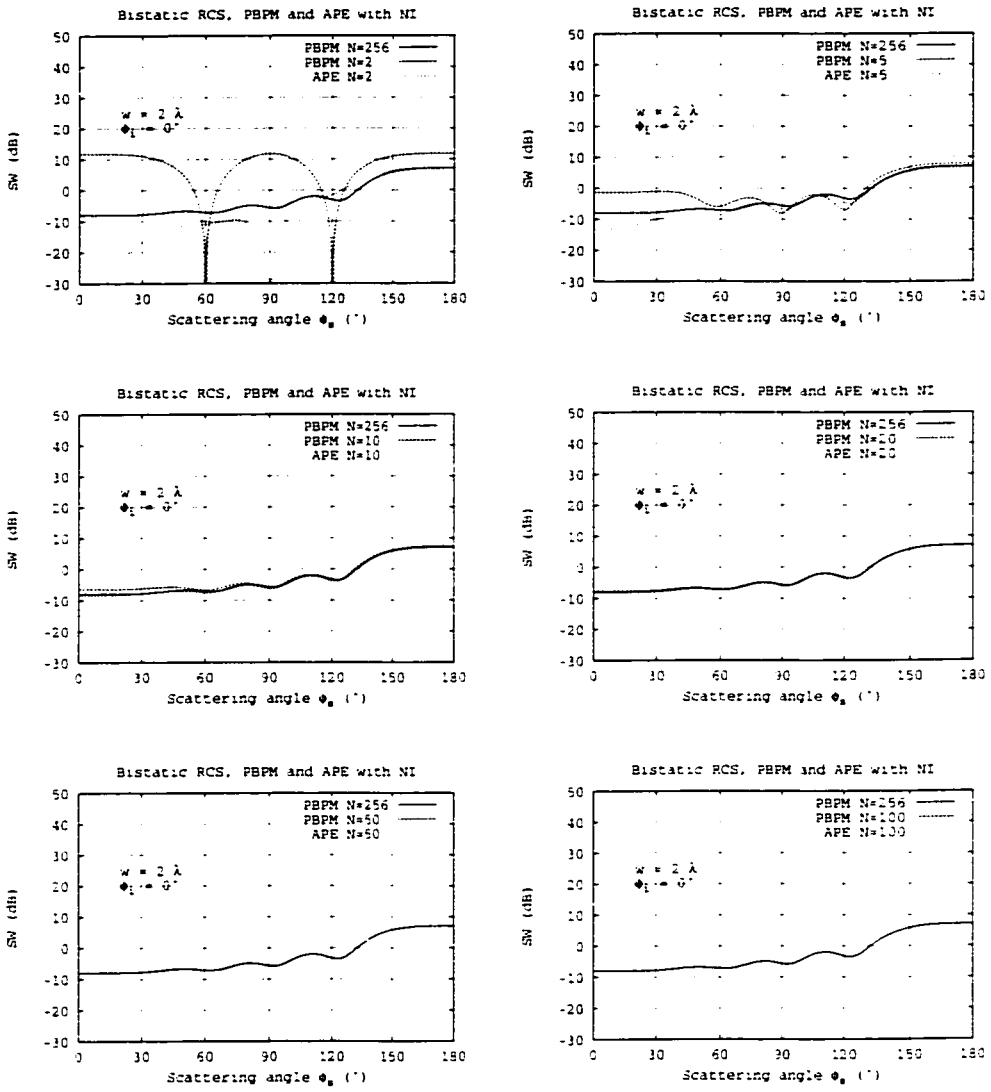


Figure 4.10: The bistatic RCS $\sigma_{\phi\phi}(\phi_s)$ of different segment numbers $N$. Comparison of PBPM and APE applying NI with 100 steps per segment. TM uniform plane wave incident upon a $2\lambda$ width strip at an angle of $\phi_i = 0^o$.

Similarly to the previous section, we can also get the results for a $20\lambda$ width strip at the same condition. They are plotted in Fig. 4.11.

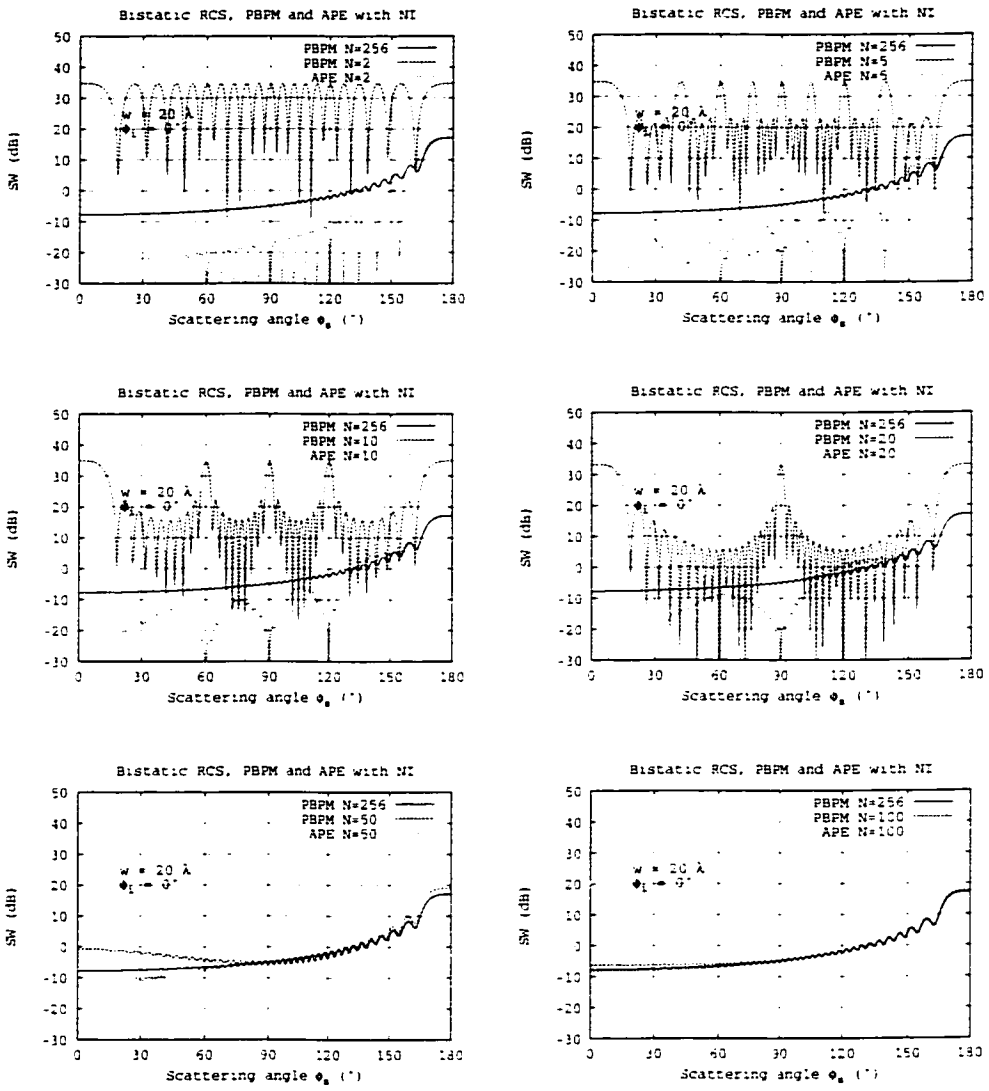


Figure 4.11: The bistatic RCS $\sigma_{\phi\phi}(\phi_s)$ of different segment numbers $N$. Comparison of PBPM and APE applying NI with 100 steps per segment. TM uniform plane wave incident upon a $20\lambda$ width strip at an angle of $\phi_i = 0^o$.

From Fig. 4.10 and Fig. 4.11, we can find that: comparing to PBPM, the APE does help RCS computation even the incident plane wave is grazing to the strip, especially at the forward scattering direction ($\phi_s = 180^o$). On the other hand, both APE and PBPM tend to be inaccurate in the backscatter direction, unless the segments length $\Delta \leq 0.2\lambda$.

# Chapter 5

# Conclusion

Studies were made for Radar Cross Section (RCS) computation by using hybrid methods.

RCS of plates was analyzed with "appendages". The goal was to develop an understanding of what happens to the RCS of a large structure (a plate) when other small obstacles are present. We examined wires, plates, plate/wire, plate/aperture, and plate/strip combinations. In all cases, a NEC-2 model, one solution of Moment Methods (MoM) code, was possible. A PO model also was used for the wire, plate/wire, and plate/aperture. The most interesting structure turned out to be the plate/strip. The strip is a small vertical blade on the flat plate. It forms a dihedral reflector and has a strong effect.

The Method of Asymptotic Phasefront Extraction (APE) was used to compute the surface current for a 2D strip, $TM_z$ case. The RCS was also obtained. It is proved that Numerical Integral (NI) is important for RCS computation when the segments are large. Excellent RCS results were observed by applying APE, using only two segments bases on a $20\lambda$ strip. This is in sharp contrast to conventional Pulse Basis Point Matching (PBPM), which would require 50 or 100 segments. The APE looks very promising and should be pursued further.

# Appendix A

# FORTRAN Code List

## A.1 plate_rcs.f90

```
PROGRAM plate_rcs
!c      Uniform plane wave was scattered by a rectangular plane
!c      incident wave in x-z plane and E-field in theta direction
!c      output scattered E-field and RCS
IMPLICIT NONE
REAL, PARAMETER :: pi = 3.141592654   ! pi
REAL, PARAMETER :: dpr = 180./pi      ! degrees per radian
COMPLEX :: es
REAL :: theta, rcs
REAL :: aa, bb, fmc, walv
INTEGER :: i                  ! loop index
aa  = 2.0                     ! length in x direction (in meter)
bb  = 1.0                     ! length in y direction (in meter)
fmc = 300.                    ! frequency f (in MHz)
wl  = 300. / fmc              ! wavelength lambda (in meter)
aa  = aa / wl                 ! length in x direction (in wavelength)
bb  = bb / wl                 ! length in y direction (in wavelength)
DO i = 0, 180                 ! observation angle theta 0 -> 90
   theta = 0.5 * i / dpr      ! degrees -> radians
   CALL sfield(aa, bb, wl, theta, theta, es, rcs)   ! monostatic
   IF (rcs < 1.5E-45) THEN
       rcs = 1.5E-45
   ENDIF
   rcs = 10. * LOG10(rcs)
   WRITE (10, *) 0.5 * i, rcs, es
END DO
END PROGRAM

SUBROUTINE sfield(ax, by, wl, thi, ths, efs, rcs)
!c      to calculate the scattered E-field and RCS
!c      Input:  AX   the length in x direction (in wavelength)
```

```
!c              BY   the length in y direction (in wavelength)
!c              WL   wavelength
!c              THI  angle theta of incident field
!c              THS  angle theta of scattered field
!c      Output: EFS  scattered E-field
!c              RCS  radar cross section
IMPLICIT NONE
REAL, INTENT(IN) :: ax, by, wl, thi, ths
COMPLEX, INTENT(OUT) :: efs
REAL, INTENT(OUT) :: rcs
REAL, PARAMETER :: pi = 3.141592654      ! pi
COMPLEX :: cj = (0.0, 1.0)
REAL :: x, sxx, sinx
wls = wl * wl
x   = pi * ax * ( SIN(thi) + SIN(ths) )  ! X=k*a*[sin(thi)+sin(ths)]/2
sxx = sinx(x)                            ! sinx(x)=sin(x)/x
efs = - cj * ax * by * wl * COS(ths) * sxx
rcs = 4. * pi * CABS(efs)**2 / wls
END SUBROUTINE sfield

REAL FUNCTION sinx(arg)
!c      to calculet sinx = sin(x) / x
IMPLICIT NONE
REAL, INTENT(IN) :: arg
REAL, PARAMETER :: epsilon = 1.0E-30
IF ( ABS(arg) > epsilon ) THEN
   sinx = SIN(arg) / arg
ELSE
   sinx = 1.
END IF
END FUNCTION sinx
```

## A.2 plate_wire.f90

```
PROGRAM plate_wire
!c      uniform plane wave scattered by a monopole on a rectangular plane
!c      incident E-field in x-z plane and in theta direction
!c      output scattered E-field and RCS
IMPLICIT NONE
REAL, PARAMETER :: pi = 3.141592654    ! pi
REAL, PARAMETER :: dpr = 180./pi       ! degrees per radian
COMPLEX :: eth, ethp, ethw1, ethw2
REAL :: aa, bb, am, sm, fmc, wavl, phi, phs, thi, theta
REAL :: smp, thip, rcs, rcsp, rcsw1, rcsw2, angle
INTEGER :: i                ! loop index
aa   = 5.                   ! plate length in x direction (in meter)
bb   = 5.                   ! plate length in y direction (in meter)
```

```
sm   = 5.                    ! wire length l (in meter)
am   = .1                    ! wire radius a (in meter)
fmc  = 300.                  ! frequency f (in MHz)
wavl = 300. / fmc            ! wavelength lambda (in meter)
aa   = aa / wavl             ! plate length ax/lambda (in wavelength)
bb   = bb / wavl             ! plate length by/lambda (in wavelength)
sm   = sm / wavl             ! wire length l/lambda (in wavelength)
am   = am / wavl             ! wire radius a/lambda (in wavelength)
phi  = 0.                    ! incident angle phi
phs  = 180.                  ! scattering angle phi
thi  = 30.                   ! incident angle theta
thip = 180. - thi            ! reflected angle theta
IF (thi < 1.) THEN
   smp = sm                  ! equivalence length for reflected field
ELSE
   smp = ABS( 0.5 * aa / TAN(thi / dpr) )
ENDIF
IF (smp > sm) THEN
   smp = sm
ENDIF
WRITE(10,*) " Incident angles theta = ", thi, " degrees"
WRITE(10,*)
WRITE(10,*) " -ANGLE-  -RCS-    -RCS-    -RCS- ", &
     &"   -RCS-       - - - E(THETA) - - -"
WRITE(10,*) "  THETA   TOTAL     MONO1    MONO2", &
     &"    PLATE     MAGNITUDE      PHASE"
WRITE(10,*) " DEGREES   DBsm      DBsm     DBsm", &
     &"    DBsm       VOLTS/M      DEGREES"
DO i = -90, 90               ! observation angle theta -90 -> 90
theta = i
CALL sfieldp(aa, bb, wavl, thi, phi, theta, phs, ethp, rcsp)
CALL sfieldw(sm, am, wavl, thi, theta, ethw1, rcsw1)
CALL sfieldw(smp, am, wavl, thip, theta, ethw2, rcsw2)
eth = ethp + ethw1 + ethw2
rcs = 4. * pi * CABS(eth)**2 / wavl**2
IF (rcs < 1.5E-45) THEN
    rcs = 1.5E-45
ENDIF
rcs   = 10. * LOG10(rcs)
IF ( rcsp < 1.5E-45) THEN
    rcsp = 1.5E-45
ENDIF
rcsp  = 10. * LOG10(rcsp)
IF ( rcsw1 < 1.5E-45) THEN
    rcsw1 = 1.5E-45
ENDIF
rcsw1 = 10. * LOG10(rcsw1)
```

```
IF ( rcsw2 < 1.5E-45) THEN
    rcsw2 = 1.5E-45
ENDIF
rcsw2 = 10. * LOG10(rcsw2)
angle = ATAN2(AIMAG(eth), REAL(eth)) * dpr
WRITE(10, 10) REAL(i), rcs, rcsw1, rcsw2, rcsp, cabs(eth), angle
10 FORMAT(1x, 5(f7.2, 2x), 1x, e13.5, 3x, f7.2)
END DO
END PROGRAM

SUBROUTINE sfieldp(ax, by, wl, thii, phii, thss, phss, eths, rcs)
!c      to calculate the scattered E-field and RCS of a rectangular plate
!c      Input:  AX    the length in x direction (in wavelength)
!c              BY    the length in y direction (in wavelength)
!c              WL    wavelength
!c              THII  angle theta of incident field
!c              PHII  angle phi of incident field
!c              THSS  angle theta of scattered field
!c              PHSS  angle phi of scattered field
!c      Output: ETHS  scattered E-field in theta direction
!c              RCS   radar cross section
IMPLICIT NONE
REAL, INTENT(IN) :: ax, by, wl, thii, phii, thss, phss
COMPLEX, INTENT(OUT) :: eths, ephs
REAL, INTENT(OUT) :: rcs
REAL, PARAMETER :: pi = 3.141592654   ! pi
REAL, PARAMETER :: dpr = 180./pi      ! degrees per radian
COMPLEX :: cj=(0.0, 1.0)
REAL :: thip, phip, thsp, phsp, wls
REAL :: x, sinx, sxx, ett
thip = thii / dpr                     ! degrees -> radians
phip = phii / dpr
thsp = thss / dpr
phsp = phss / dpr
wls  = wl * wl
x    = pi * ax * (SIN(thip) * COS(phip) + SIN(thsp) * COS(phsp))
sxx  = sinx(x)                        ! sxx=sin(X)/X
ett  = COS(thsp) * COS(phip - phsp)
eths = -cj * ax * by * wl * ett * sxx
rcs  = 4. * pi * CABS(eths)**2 / wls
END SUBROUTINE sfieldp

SUBROUTINE sfieldw(l, a, wl, thii, thss, efs, rcs)
!c      to calculate the scattered E-field and RCS of a thin wire
!c      Input:  L     the length of the wire (in wavelength)
!c              A     the radius of the wire (in wavelength)
!c              WL    wavelength
```

```
!c              THI  angle theta of incident field
!c              THS  angle theta of scattered field
!c      Output: EFS  scattered E-field
!c              RCS  radar cross section
IMPLICIT NONE
REAL, INTENT(IN) :: l, a, wl, thii, thss
COMPLEX, INTENT(OUT) :: efs
REAL, INTENT(OUT) :: rcs
REAL, PARAMETER :: pi = 3.141592654   ! pi
REAL, PARAMETER :: dpr = 180./pi      ! degrees per radian
COMPLEX :: cj=(0.0, 1.0), cfac
REAL :: thiw, thsw, wls, u, sxu, sinx, rfac
thiw = thii / dpr
thsw = thss / dpr
wls  = wl * wl
IF ((thiw < 1. / dpr) .OR. (ABS(thiw - pi) < 1. / dpr)) THEN
   efs = 0.
ELSE
   u    = pi * l * (COS(thiw) + COS(thsw))
   sxu  = sinx(u)                      ! sinx(u)=sin(U)/U
   rfac = L * wl * SIN(thsw) * sxu / SIN(thiw)
   cfac = pi * cj / 2 + LOG((1.781 * pi * a) * SIN(thiw))
   efs  = 0.5 * rfac / cfac
ENDIF
rcs = 4. * pi * CABS(efs)**2 / wls
END SUBROUTINE sfieldw

REAL FUNCTION sinx(arg)
!c      to calculet sinx = sin(x) / x
IMPLICIT NONE
REAL, INTENT(IN) :: arg
REAL, PARAMETER :: epsilon = 1.0E-30
IF ( ABS(arg) > epsilon ) THEN
   sinx = SIN(arg)/arg
ELSE
   sinx = 1.
END IF
END FUNCTION sinx
```

# Bibliography


[1] C. A. Balanis, *Advanced Engineering Electromagnetics.* John Willy & Sons Inc., 1989.

[2] J. Moore and R. Pizer, *Moment Methods in Electromagnetics.* Research Studies Press, 1984.

[3] R. F. Harrington, *Field Computation by Moment Methods.* Macmillan, New York, 1968.

[4] S. L. Ray, A. F. Peterson and R. Mittra, *Computational Methods For Electromagnetics.* The IEEE/OUP Series on Electromagnetic Wave Theory. IEEE Press. 1998.

[5] G. J. Burke and A. J. Poggio, *NEC-2 Manual. Part III: User's Guide.* Lawrence Livermore Laboratory, Livermore, California.

[6] P. Beckmann, *The Depolarization of Electromagnetic Waves.* The Golem Press. Boulder, Colorado, 1968.

[7] R. Paknys and L. Wang, *RCS Prediction Using High Frequency Techniques.* ECE Department of Concordia University. Final Report Prepared for DREO Contract W7714-990339. March 31, 2002.

[8] R. Paknys and L. Wang, *RCS Prediction Using High Frequency Techniques.* ECE Department of Concordia University. Quarterly Report Prepared for DREO Contract W7714-990339. June 30, October 15, December 18, 2002.

[9] D.-H. Kwon, R. J. Burkholder, and P. H. Pathak, *"Efficient method of moments formulation for large PEC scattering problems using Asymptotic Phasefront Extraction (APE),"* IEEE Trans. on Antennas and Propagations. Vol. 49, pp. 593-591, April 2001.

[10] Johan Edlund, *A Parallel, Iterative Method of Moments and Physical Optics Hybrid Solver for Arbitrary Surfaces.* Master's Thesis. Uppsala University, Sweden, 2001.

[11] J. H. Richmond, *"Radiation and scattering by thin wire structures in a homogeneous conducting medium,"* IEEE Trans. on Antennas and Propagations. March 1974

[12] K. Aberegg and A. F. Peterson, *"Application of the integral equation asymptotic phase method of two-dimensional scattering,"* IEEE Trans. on Antennas and Propagations. Vol. 43, pp.534-537, May 1995.

[13] H. Liu. *Scattering from Periodic Array of Parallel Strips.* PhD Thesis, Concordia University, Canada, 2001.

[14] S. J. Chapman, *Fortran 90/95 for Scientists and Engineers.* First Edition. WCB/McGraw-Hill, 1998.

[15] Erwin Kreyszig, *Advanced Engineering Mathematics.* 8th Edition. John Willy & Sons Inc. 1999.